Systems/Circuits

Synapse-Specific Trapping of SNARE Machinery Proteins in the Anesthetized *Drosophila* Brain

Adam D. Hines,[1] Amber B. Kewin,[1] Matthew N. Van De Poll,[1] Victor Anggono,[1,2] Adekunle T. Bademosi,[1,2] and Bruno van Swinderen[1]

[1]Queensland Brain Institute, The University of Queensland, St Lucia 4072, Queensland, Australia and [2]Clem Jones Centre for Ageing and Dementia Research, The University of Queensland, St Lucia 4072, Queensland, Australia

General anesthetics disrupt brain network dynamics through multiple pathways, in part through postsynaptic potentiation of inhibitory ion channels as well as presynaptic inhibition of neuroexocytosis. Common clinical general anesthetic drugs, such as propofol and isoflurane, have been shown to interact and interfere with core components of the exocytic release machinery to cause impaired neurotransmitter release. Recent studies however suggest that these drugs do not affect all synapse subtypes equally. We investigated the role of the presynaptic release machinery in multiple neurotransmitter systems under isoflurane general anesthesia in the adult female *Drosophila* brain using live-cell super–resolution microscopy and optogenetic readouts of exocytosis and neural excitability. We activated neurotransmitter-specific mushroom body output neurons and imaged presynaptic function under isoflurane anesthesia. We found that isoflurane impaired synaptic release and presynaptic protein dynamics in excitatory cholinergic synapses. In contrast, isoflurane had little to no effect on inhibitory GABAergic or glutamatergic synapses. These results present a distinct inhibitory mechanism for general anesthesia, whereby neuroexocytosis is selectively impaired at excitatory synapses, while inhibitory synapses remain functional. This suggests a presynaptic inhibitory mechanism that complements the other inhibitory effects of these drugs.

Key words: *Drosophila*; general anesthesia; neurotransmitter; optogenetics; super-resolution microscopy; syntaxin1a

---

Significance Statement

General anesthetics are promiscuous drugs that act on a variety of presynaptic and postsynaptic proteins. Yet they produce a common endpoint—loss of behavioral responsiveness—in all animals. Using optogenetic techniques to measure functional readouts in identified neurons in the *Drosophila* brain, we have found that the volatile anesthetic isoflurane impairs neurotransmitter release from excitatory synapses and that this is associated with the immobilization of release machinery proteins. Inhibitory synapses were unaffected. This suggests a level of presynaptic specificity to the anesthetic's mechanism of action which complements the other known effects on synaptic function and potentially explains how some of these drugs might work to produce the common endpoint termed general anesthesia.

Introduction

General anesthesia is a reversibly induced state of unconsciousness and unresponsiveness that has been used clinically for over 150 years. It has been understood for over four decades

that these drugs interact with proteins in the central nervous system (CNS) to disrupt neuronal activity and silence wake-promoting circuits (Franks, 2008). The best-characterized interaction involves the potentiation of postsynaptic chloride-permeable γ-aminobutyric acid type A ($GABA_A$) receptors, which act to hyperpolarize wake-promoting neurons and thus promote a sleep-like state (Franks and Lieb, 1984; Jones et al., 1995; Kim et al., 2020). However, such postsynaptic effects cannot fully account for the depth and complexity of general anesthesia (Zecharia et al., 2012; Lor et al., 2020) nor the succession of distinct behavioral endpoints or the prolonged recovery time required for some drugs, especially the volatile agents (Cylinder et al., 2024). Accordingly, other protein targets of general anesthetics have been discovered, especially at the presynapse, including ion channels (Bertaccini et al., 2014; Ton et al., 2017; Koyanagi et al., 2019; Torturo et al., 2019; Zhou et al., 2019),

kinesins (Bensel et al., 2017; Woll et al., 2018), mitochondria (Morgan et al., 2002; Jung et al., 2022; Perouansky et al., 2023), and the synaptic release machinery (van Swinderen et al., 1999; Herring et al., 2009, 2011; Xie et al., 2013; Zalucki et al., 2015; Bademosi et al., 2018b; Troup et al., 2019; Karunanithi et al., 2020; Hines and van Swinderen, 2021). Although it is known that general anesthetics impair neurotransmitter release and neuronal communication (Herring et al., 2009, 2011; Bademosi et al., 2018b; Karunanithi et al., 2020; Wang et al., 2020; Speigel and Hemmings, 2021), the relative contribution of these different presynaptic targets remains unclear.

The soluble N-ethylmaleimide-sensitive factor attachment protein receptor (SNARE) complex, which comprises syntaxin1a (Sx1a), SNAP25, and VAMP2, is essential for neurotransmitter release (Südhof, 2012). These proteins form a tetramer of tight α-helical structure that facilitates the docking and fusion of synaptic vesicles with the plasma membrane. Sx1a has been shown in multiple studies to be a target of different general anesthetics, both volatile and intravenous (van Swinderen et al., 1999; Herring et al., 2009, 2011; Bademosi et al., 2018b; Karunanithi et al., 2020; Hines and van Swinderen, 2021). In the presence of a general anesthetic, Sx1a molecules are hypothesized to be trapped into nonfunctional nanoclusters on the presynaptic membrane, potentially preventing them from forming competent SNARE complexes (Bademosi et al., 2018b; Hines and van Swinderen, 2021). Whether this effect on Sx1a is observed in all synapses is unknown. Furthermore, it is unclear whether general anesthetics also trap other release machinery proteins into nonfunctional nanoclusters at the presynapse.

In this study, we sought to determine the effects of a volatile anesthetic (isoflurane) on neuroexocytosis and Sx1a function in different neurotransmitter systems (cholinergic, GABAergic, and glutamatergic) in the intact brain tissue. Using an ex vivo brain preparation of the *Drosophila* fruit fly as a model (Hines and van Swinderen, 2021), we conducted optogenetically induced neuroexocytosis assays (Miesenböck et al., 1998) and single-molecule imaging (Zhang et al., 2012) to study how the diffusion and clustering of Sx1a correlate with vesicle release dynamics at different synapses from identified mushroom body output neurons (MBONs). We found that in conjunction with impaired synaptic release, Sx1a molecules become more immobilized in both synaptic and extrasynaptic compartments of cholinergic MBONs under isoflurane anesthesia, but only Sx1a proteins at synapses were entrapped into clusters. In contrast, we saw no change in exocytosis or Sx1a diffusion dynamics under isoflurane general anesthesia in two putative inhibitory MBONs. Notably, isoflurane had no significant effect on MBON excitability, as measured by a calcium reporter. Together, this suggests a synapse-specific effect in excitatory neurons.

Materials and Methods

Transgenic fly strains. UAS-Sx1a-mEos3.2 and UAS-Rop-mEos3.2 constructs for super-resolution microscopy were generated as previously described (Bademosi et al., 2018a). In brief, *Drosophila* Sx1a and Rop had an mEos3.2 fluorophore attached to them by replacing the stop codon for a linker with the sequence gaggtaccgcgggcccgggatccaccg. Synthesis and cloning of this construct were performed by VectorBuilder, and it was cloned into a 5xUAS Hsp70 *Drosophila* expression vector with a miniwhite gene. PhiC31 integration into the *Drosophila* genome was performed by GenetiVision into the attP40 landing site on the second chromosome.

Fly stocks. All flies used in the study were reared on a standard yeast–sugar–agar media (1.0;1.5;0.5 g ratio) food at 25°C with a 12 h day/night cycle. Flies used for the CsChrimson stimulation were reared on the same food supplemented with 0.2 mM all-trans retinal (ATR) for at least 72 h prior to imaging. w1118 UAS-Sx1a-mEos3.2/Cyo; Sb/Tm6Tb and w1118 UAS-Rop-mEos3.2/Cyo; and Sb/Tm6Tb stocks were combined with w1118 Sco/Cyo; UAS-CsChrimson-mVenus/Tm6Tb to generate the working strains w1118 UAS-Sx1a-mEos3.2/Cyo; UAS-CsChrimson-mVenus/Tm6Tb and w1118 UAS-Rop-mEos3.2/Cyo; and UAS-CsChrimson-mVenus/Tm6Tb to cross to split-Gal4 drivers. w1118 UAS-GCaMP6s and sb/Tm6Tb stocks were combined with w1118 Sco/Cyo; UAS-CsChrimson-mCherry/Tm6Tb to generate the working strain w1118 UAS-GCaMP6s/Cyo; and UAS-CsChrimson-mCherry to cross to split-Gal4 drivers. MBON split-Gal4 lines have been previously described (Aso et al., 2014) and were ordered from the Bloomington *Drosophila* Stock Centre. For all single-particle tracking photoactivated localization microscopy (sptPALM) experiments after expressing the working strain into a split-Gal4, female flies were sorted upon eclosing by brief anesthetization on a CO_2 pad and imaged 3–5 d later. Females were chosen to control for sexual dimorphisms in expression patterns.

Adult Drosophila *brain dissection and mounting.* Three- to five-day-old adult *Drosophila* brains were prepared for imaging similarly as previously described (Hines and van Swinderen, 2021). From the baseline to CsChrimson activation experiments, flies were cold anesthetized by placing them in a glass, air-tight chamber on ice for 30 s, then dissected on ice-cold PBS, and imaged immediately. For all anesthesia experiments, flies were placed in a glass, air-tight chamber and exposed to either 5 μl air (control) or 100% isoflurane (equivalent to a 1.5% concentration) for 15 min prior to cold anesthetization and dissection, as determined by gas chromatography (Zalucki et al., 2015). For the isoflurane condition, the 15 min started after the flies became fully anesthetized (i.e., were behaviorally unresponsive to mechanical stimulation at the base of the glass chamber), which on average took ~10–30 s per fly.

The imaging buffer was a modified hemolymph-like 3.1 (HL3.1; Feng et al., 2004) solution which consisted of 70 mM NaCl, 5 mM KCl, 1.5 mM $CaCl_2$, 2 mM $MgCl_2$, 5 mM HEPES, 115 mM sucrose, 5 mM trehalose, and pH adjusted to 7.2 with $NaHCO_3$ (Sigma-Aldrich). Imaging buffer was made in batches, aliquoted, and stored at −80°C. A fresh aliquot of HL3.1 was defrosted for each day of experiments. Dissected brains are placed in 2 μl of imaging buffer on a glass slide and sealed underneath a No. 1.5 22 × 22 mm cover glass rimmed with vacuum grease and nail polish.

Live-cell synaptopHluorin imaging and processing. Prior to imaging, we bleached the baseline synaptopHluorin fluorescence using 25% power of an 18.72 mW 488 nm laser at 30 ms exposure for 1 min. This is because there is a significantly high background fluorescence of synaptopHluorin in the *Drosophila* nervous tissue, potentially due to a higher internal vesicle pH compared with mammalian systems. Photobleaching reduced the amount of existing synaptopHluorin on the plasma membrane, without affecting synaptopHluorin molecules on synaptic vesicles that are yet to be exocytosed—thereby improving the signal-to-noise ratio. After the photobleaching, the exposure time was set to 100 ms, and 488 nm laser power reduced to 4% to capture synaptopHluorin release. The 10 s of the baseline was captured prior to 2 min of 10 Hz red-light stimulation using 25% power of a 20.6 mW 568 nm laser. Recovery was captured for 5 min after red-light stimulation.

To analyze the data, we applied several preprocessing steps to the raw imaging data to resolve the true delta fluorescence change during stimulation. Firstly, recordings were truncated to just include the first 500 frames of the recovery condition while retaining the full-length baseline and stimulation conditions to allow for more accurate motion correction. The truncated recordings were motion corrected using ImageJ's "Correct 3D Drift" plugin (Parslow et al., 2014) with "Correcting only x & y," "Multi-time scale computation," and "Sub pixel drift correction" all selected. All other settings were left to default. Motion-corrected recordings were background subtracted to a rolling ball radius of 5 pixels (0.5 μm). To eliminate baseline fluorescence, a maximum *Z*-projection of the first 100 frames (baseline prior to red-light activation) was generated and used to subtract all the pixel values for the entire recording. Finally, a despeckle noise remover was applied to eliminate background signal incurred due to bleed-through of red light into the camera

detector. To select regions of interest (ROIs) to analyze, we generated a standard deviation Z-projection of the processed recording, and we calculated a "Li" autothreshold to create a mask and selection of the regions with high increases of fluorescence. The selection was then applied to the recording, and a multimeasure of the mean pixel gray value and area for each individual ROI was generated and analyzed in Python. These pre-processing steps were crucial to see the true change in fluorescence throughout stimulation.

Quantification of synaptopHluorin release. Mean gray values and areas measured in each ROI for SynaptopHluorin release were imported into a custom Python script for analysis (available at github.com/AdamDHines/synaptopHluorin-analysis). The fluorescence ($F - F_0$) for each ROI of a recording was summed together and divided by the total area of release for the "total relative fluorescence." The data was down-sampled by averaging the total relative fluorescence into 10 s bins over the course of the 2 min stimulation period. To calculate a proxy for quantal release, we calculated a trapezoidal area under the curve (AUC) for each of the total relative fluorescence curves for the "total relative activity." The relative ROI density was calculated by taking the number of detected ROIs and dividing it by the total area of the imaged neuron. This was calculated by taking an image of the neuron using 488 nm excitation, background subtracting with a 0.5 μm rolling ball radius, and applying a "Li" autothreshold to create a mask around the neuron (Li and Tam, 1998). This mask was converted to a selection, and the total area was calculated.

Release area groups were calculated using the k-means clustering of 470 ROIs from the control acetylcholine recordings. A maximum of 10 iterations and three groups was defined, which repeatedly output the same cluster centroids. The centroids were then used to discretize the ROIs for all synaptopHluorin recordings into small, medium, or large groups and analyzed the same way as the total activity.

Drosophila brain PALM. The method for performing sptPALM in adult fly brains has been extensively described (Hines and van Swinderen, 2021). All super-resolution microscopy was done on a Zeiss ELYRA PS.1 to allow simultaneous 405 and 561 nm wavelength laser operation microscope through an Apochromat 100× 1.4 NA oil immersion objective. All recordings were captured on an iXon EMCCD camera. ROIs were navigated to with a 10× 0.45 NA Plan-Apochromat objective using a 488 nm wavelength laser before switching to 100× oil immersion. Brains were illuminated in a highly inclined and laminated optical sheet imaging mode with an angle of 47.3° to improve the signal-to-noise ratio. A 0.02–0.08% power of a 0.6 mW 405 nm laser was used to photoconvert mEos3.2 from green to red, and 25% power of a 20.6 mW 561 nm laser was used to excite photoconverted mEos3.2 molecules. A Zeiss incubation chamber with a TempModule S attached to it regulated the temperature at 25°C for all imaging experiments. The 32,000 images were captured at a 30 ms exposure time (the lowest possible for the camera to record at) per recording, with ~1–2 ms between each frame.

Single-particle tracking of PALM data. Molecule localization and tracking were performed in the custom MATLAB GUI *Single Particle Analysis* which employs the free ImageJ plugin TrackMate (Tinevez et al., 2017; Hines and van Swinderen, 2021). Single Sx1a-mEos3.2 and Rop-mEos3.2 molecules were detected and localized using a Laplacian of Gaussian detection algorithm (Eq. 1) with a spot radius of 0.4 μm and a variable threshold depending on the signal-to-noise ratio (manually determined). Detection was improved by using median filtering and subpixel localization. We achieved a localization precision of ~25 nm with a point spread function half-width of 134 nm as follows:

$$g(x, y, t) = \frac{1}{2\pi t} e^{-\frac{x^2 + y^2}{2t}}, \tag{1}$$

where x and y are the spatial coordinates and t is the frame time. Molecule tracking between frames was performed by a linear assignment problem algorithm (Jaqaman et al., 2008). To be included for analysis, a track had to have a minimum 6 spots and a maximum of 1,000 per

trajectory. Every trajectory represents the movement of a single mEos3.2-tagged molecule.

Mean-squared displacement (MSD) and clustering analysis were all performed using the segNASTIC software (Wallis et al., 2023). For accurate spatiotemporal clustering analysis, drift correction was applied to the x and y coordinates of trajectories by feeding drift tables in Zeiss ZEN PALM calculated by a model-based drift algorithm. Drift correction did not change the mobility data but did give different results for spatiotemporal clustering indicating the importance of performing drift correction in this analysis. The AUC was calculated in GraphPad Prism 9 with a baseline starting at $Y = 0$, ignoring peaks that are <10% of the distance from minimum to maximum Y and defining that all peaks must go above the baseline. Outliers in MSD data were determined by excluding results that were ±2 times the standard deviation of the mean AUC for each condition. Outliers for clustering data were determined by the ROUT method with a maximum false discovery rate of 1% calculated in GraphPad Prism 9.

GCaMP6s imaging. Neural excitability was measured using a cytosolic GCaMP6s (Troup et al., 2023), utilizing the same microscope infrastructure and following the same optogenetic activation protocol as for the synaptopHluorin experiments above. MBONs were visualized and activated using CsChrimson-mCherry. The 488 nm laser power was set to 4% for 100 ms exposure, and the 568 nm laser was set to 25% power for 100 ms exposure, with 4,300 frames recorded per experiment. Drift correction, ROI identification, and baseline normalization were applied as for the synaptopHluorin experiments. A small red-light imaging artifact was removed from all experiments, by subtracting an average trace displayed by −ATR control flies where CsChrimson had not been activated. Resulting fluorescence traces were analyzed using a custom MATLAB software, and statistical analyses were performed in GraphPad Prism 9.

Confocal imaging and image processing. All confocal imaging was performed on a W1 Yokogawa spinning disk attached to a Zeiss Axio Observer Z1 controlled by the Slidebook 6.0 software. For colocalization imaging of synaptopHluorin and CsChrimson-mCherry, a 20× 0.8 NA Plan-Apochromat and 40× 1.2 NA C-Apochromat water immersion objective were used to image neural structures. mVenus and synaptopHluorin were excited with a 488 nm laser wavelength. All images were captured on a Hamamatsu ORCA-Flash 4.0 V2 scientific complementary metal-oxide-semiconductor camera.

Data and statistical analysis. Data is presented as the mean ± the standard error of the mean (SEM). Individual data points indicate single recordings from multiple brains. For all synaptopHluorin and sptPALM experiments, recordings were taken on both the left- and right-hand side of the brain due to the bilateral expression patterns in the split-Gal4 lines. Statistical analysis tests for significance were t tests (Mann–Whitney U test) and one-way ANOVA, performed in GraphPad Prism 9 and Python with the SciPy package. Mann–Whitney U tests included the calculation of the effect size (rank biserial correlation, r) as defined by the following:

$$r = 1 - \left(\frac{2 \cdot U}{n1 \cdot n2} \right),$$

where U is the Mann–Whitney U statistic and $n1/n2$ are the sample sizes of the two groups being compared. ANOVA analysis statistics include corresponding F values. A significance threshold of 0.05 was employed for all statistical analysis. All nonsignificant results are reported as ns.

Results

Isoflurane impairs synaptic vesicle exocytosis in the fly brain

To establish the effects of general anesthesia in the *Drosophila* brain, we administered the volatile agent isoflurane to adult flies to induce unconsciousness and a loss of behavioral responsiveness. Flies were exposed to either a 1.5 vol% concentration of isoflurane (Zalucki et al., 2015) or air as a control for 15 min, before brain dissection and imaging (Fig. 1A). We imaged in
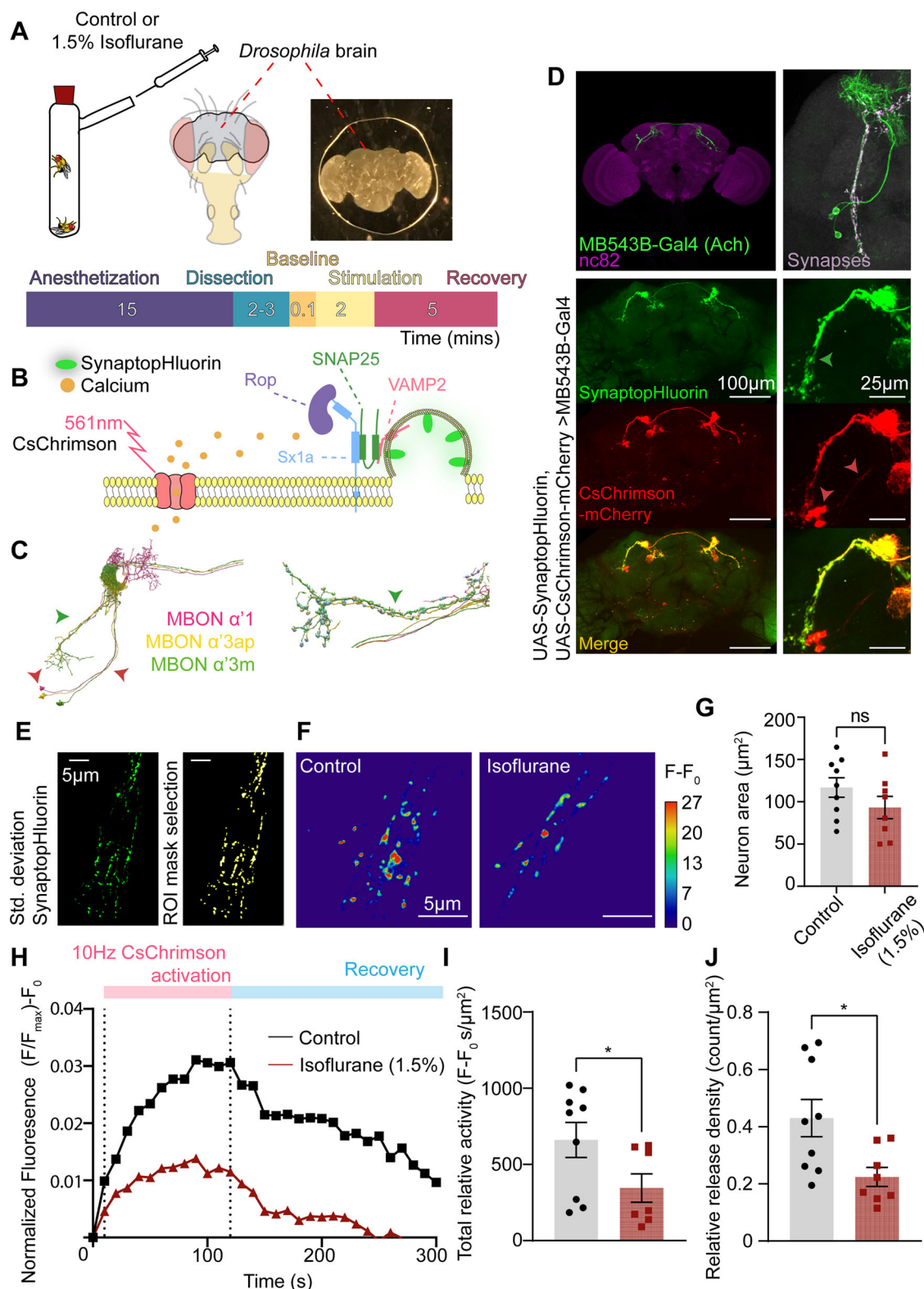
Figure 1. Isoflurane impairs neuroexocytosis at cholinergic synapses in the adult *Drosophila* brain. *A*, Isoflurane anesthesia, equivalent to a 1.5% concentration, was induced in female *Drosophila* flies in an air-tight chamber for 15 min. The control condition consisted of only air. Brains were then dissected and mounted and imaged using a standard protocol of 10 s baseline, 2 min stimulation, and 5 min recovery. *B*, Schematic of synaptopHluorin activity in response to calcium-triggered SNARE-mediated release via CsChrimson activation. *C*, Neural skeleton of MB543B-Gal4 derived from FIB-SEM *Drosophila* brain volume (left) with a close-up of the synapses (right). Green arrow matches synaptopHluorin expression in *D*. *D*, MB543B-Gal4 expression pattern in the *Drosophila* brain immunostained for the presynaptic marker bruchpilot (nc82), image taken from Janelia FlyLight split-Gal4 collection. Confocal images of UAS-synaptopHluorin (top), UAS-CsChrimson-mCherry (middle), and their overlap (bottom) expressed in the cholinergic split-Gal4 (MB543B-Gal4). SynaptopHluorin expression is enriched in synapses (green arrow) but not in cell bodies or extrasynaptic compartments (red arrows). *E*, Standard deviation *Z*-projection of the synaptopHluorin fluorescence change observed during CsChrimson activation (left). An ROI selection is applied to individual release sites for analysis (right). *F*, Comparison of synaptopHluorin fluorescence changes under control (left) or isoflurane (right) during CsChrimson activation. Isoflurane decreases the density of release areas and peak fluorescence from the baseline. *G*, The average total neuron area between control and isoflurane conditions was not significantly
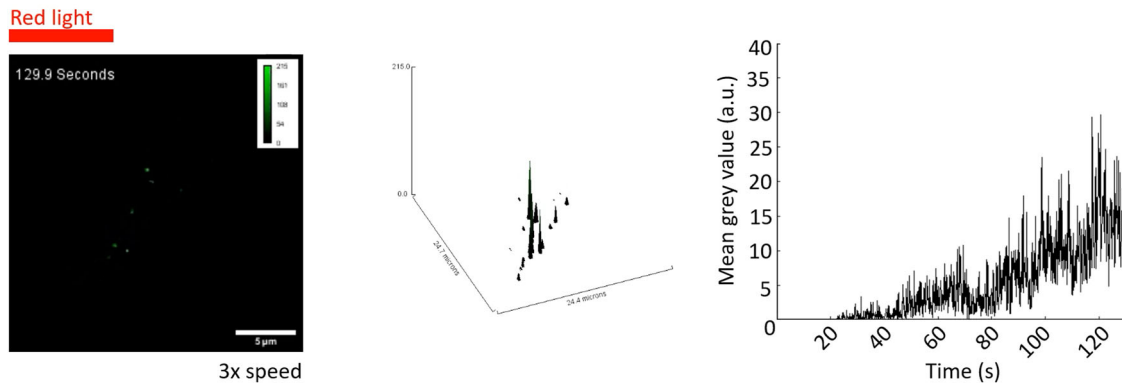
Movie 1. (Associated with Fig. 1). Recording synaptopHluorin activity from cholinergic synapses in the *Drosophila* brain. Left, Example of the processed imaging experiments with synaptopHluorin, highlighting the true delta fluorescence of release activity during CsChrimson activation. Middle, A surface plot of the processed recordings, highlighting the restriction of activity to individual synaptopHluorin ROIs. Right, A trace curve of fluorescence activity being measured for all detected ROIs. [view online]

physiological HL3.1 solution (Feng et al., 2004) which has a high sugar content to promote tissue health and which results in identifying effects not dependent on metabolic effects of anesthetics (Jung et al., 2022). To quantify synaptic vesicle exocytosis, we used synaptopHluorin, a pH-sensitive reporter of vesicle fusion to the plasma membrane (Miesenböck et al., 1998; Fig. 1B). We expressed the synaptopHluorin in MBONs (Aso et al., 2014), by selecting MBON split-Gal4s to drive the transgene expression in specific MBON subsets that have been mapped to different neurotransmitter systems (cholinergic, GABAergic, glutamatergic, etc.) by the *Drosophila* hemibrain connectome (Scheffer et al., 2020). We focused on MBONs in this study because they provided neurotransmitter specificity as well as an accessible presynaptic architecture. We started with a set of cholinergic MBONs by using the MB543B split-Gal4 driver (Fig. 1C,D), as the major excitatory neurotransmitter system in the fly brain is cholinergic (Gu and O'Dowd, 2006). To stimulate synaptic release, we coexpressed the Ca^{2+}-permeable channelrhodopsin CsChrimson tagged with mCherry and activated with red-light exposure (Fig. 1B). SynaptopHluorin was strongly expressed in synapses but not extrasynaptic areas or cell bodies, whereas CsChrimson expression was evident throughout the entire neuron (Fig. 1D). All neurons were subjected to a standardized imaging protocol of a 10 s baseline, 2 min of 10 Hz CsChrimson activation, and 5 min of recovery poststimulation (Fig. 1A, timeline; Movie 1). We uncovered dynamic clusters of synaptopHluorin signal by identifying ROIs (Fig. 1E) using a series of image preprocessing steps (see Materials and Methods, Live-cell synaptopHluorin imaging and processing). We found that isoflurane exposure impaired the density and intensity of synaptopHluorin release at these cholinergic synapses (Fig. 1F). However, this was not due to changes in the average imaged area (Fig. 1G). Rather, the total relative activity (amount of synaptopHluorin release per total release area) and ROI density (the number of ROIs per total neuron size) were significantly decreased under isoflurane anesthesia (Fig. 1H–J). Since recovery dynamics appeared similar under isoflurane

(Fig. 1H), we focus only on the excitation segment in our subsequent analyses. In summary, isoflurane impairs evoked cholinergic neurotransmission and reduces the density of synaptopHluorin signal in this specific MBON in the adult *Drosophila* brain.

Previous research on fly larval motoneurons found that the intravenous general anesthetic propofol differentially impaired transmitter release at active zones of varying size (Karunanithi et al., 2020). Propofol halved the total release from all motoneuron synapses; however, larger synapses were less impaired than smaller ones due to their greater number of active release sites (Karunanithi et al., 2020). To examine whether isoflurane was affecting all release sites equally in these cholinergic brain synapses, we classified ROI based on their size to observe if there were any differences (Fig. 2A). ROIs were defined as either small (<0.08 μm²), medium (0.09–0.42 μm²), or large (>0.43 μm²) based on the *k*-means clustering of 470 release areas from the control condition (Fig. 2A; see Materials and Methods, Quantification of synaptopHluorin release). When looking at just the average fluorescence from each release size group for both control and isoflurane conditions, all ROIs show a continuous increase in synaptopHluorin release over time, with large ROIs contributing the greatest amount of fluorescence, indicating that they are releasing more neurotransmitter than the small or medium groups (Fig. 2B). However, when looking at the absolute number and relative frequency of each release group, we find that most of the ROIs fall within the small and medium category (Fig. 2C). The bulk of the total activity from these cholinergic synapses then are contributed to predominantly by small and medium ROIs (<0.42 μm², Fig. 2C). Isoflurane does not alter the distribution of different ROI sizes, with no significant difference in either the absolute count or relative frequency of small, medium, and large ROIs (Fig. 2C). Finding that small and medium synapses contributed relatively more to cholinergic release prompted us to investigate if the total relative activity (see Materials and Methods, Quantification of synaptopHluorin release) within each synapse size group was diminished. When

←

different (n = 9 control; n = 8 isoflurane; p = 0.277; rank biserial correlation, r = −0.33; Mann–Whitney *U* test; ±SEM). **H**, Activity traces of synaptopHluorin release in control (black) and isoflurane (red) conditions during and after CsChrimson activation, normalized to the baseline and averaged over 10 s segments. Each trace is from a different fly. **I**, Total relative activity (average change in fluorescence per μm²) was significantly decreased under isoflurane anesthesia (p = 0.022; rank biserial correlation, r = −0.68; Mann–Whitney *U* test, ±SEM). **J**, In addition to decreased release, the density of release sites (number of ROIs relative to total neuron area in μm²) was significantly decreased under isoflurane anesthesia (p = 0.0206; rank biserial correlation, r = −0.667; Mann–Whitney *U* test; ±SEM).
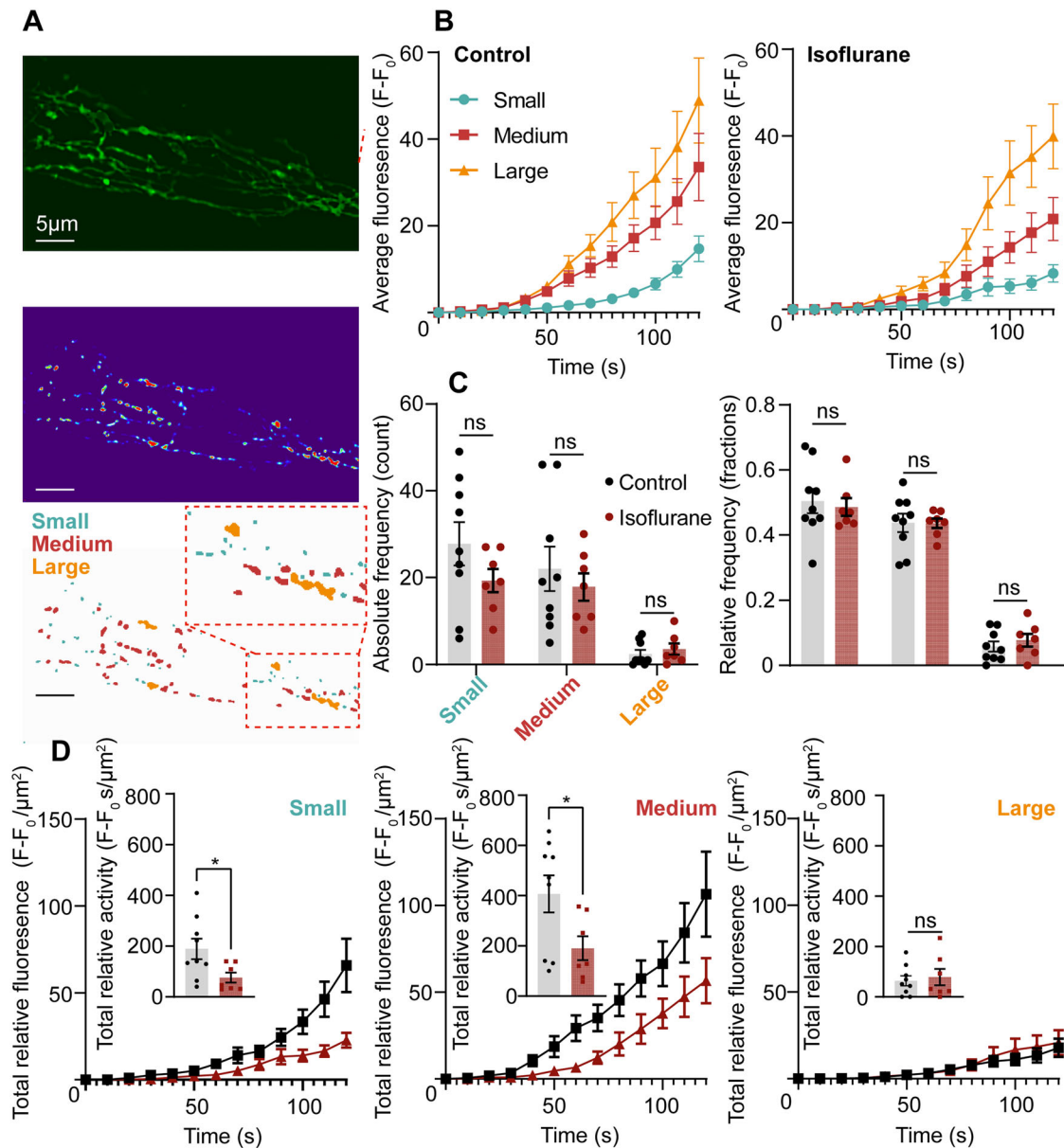
Figure 2. Isoflurane affects release from smaller but not larger active zones. *A*, Top, Baseline fluorescence of synaptopHluorin in cholinergic synapses with (middle) the standard deviation of release during CsChrimson activation. Bottom, Classification of release sites into small (<0.08 μm²), medium (0.09–0.42 μm²), and large (>0.43 μm²). Classifications based on *k*-means clustering of individual release areas (scale bar, 5 μm). *B*, Average fluorescence traces normalized to the baseline for the control (left) and isoflurane (right) for each of the different release area groups. No significant difference in the activity between the control and isoflurane for each group. *C*, Frequency of each release group between control and isoflurane showed no significant difference in the absolute number of groups within each condition (absolute, small, $F_{(1,18)} = 1.89$; $p = 0.19$; medium, $F_{(1,18)} = 0.41$; $p = 0.53$; large, $F_{(1,18)} = 0.53$; $p = 0.48$) or the relative frequency (relative, small, $F_{(1,18)} = 0.07$; $p = 0.80$; medium, $F_{(1,18)} = 0.01$; $p = 0.94$; large, $F_{(1,18)} = 0.15$; $p = 0.70$; ANOVA). All data ± SEM. *D*, Relative activity for small (left), medium (middle), and large (right) release groups. Only the small and medium release groups showed a significant decrease in activity between control and isoflurane conditions (small, $t_{(14)} = 2.48$; $p = 0.0339$; medium, $t_{(14)} = 2.38$; $p = 0.039$). The large release group did not show a significant difference in activity (large, $t_{(14)} = 0.085$; $p = 0.934$; ANOVA). All data ± SEM.

comparing the total relative activity of each group, we observed a significant reduction in release only from the small and medium groups and no change in the large ROIs (Fig. 2D). This indicates that disruptions to neurotransmission depend on the size or architecture of a synapse, with the smaller synapses being more vulnerable to isoflurane presumably due to fewer active zones (Karunanithi et al., 2020), lower amounts of presynaptic proteins to support them (Ullrich et al., 2015), or less metabolic support (Jung et al., 2022). We next turned our attention to components of the active zone architecture to investigate presynaptic proteins likely to be key targets of isoflurane.

Synaptic release machinery proteins are disrupted by isoflurane

General anesthetics disrupt synaptic transmission through a variety of mechanisms (Hemmings et al., 2019). One proposed mechanism involves the protein machinery that controls neurotransmitter release (Herring et al., 2009, 2011; Xie et al., 2013; Zalucki et al., 2015; Bademosi et al., 2018b; Troup et al., 2019; Hines and van Swinderen, 2021), including a member of the SNARE complex Sx1a (Nagele et al., 2005; Bademosi et al., 2018b; Hines and van Swinderen, 2021). To understand how isoflurane might disrupt Sx1a function in cholinergic synapses
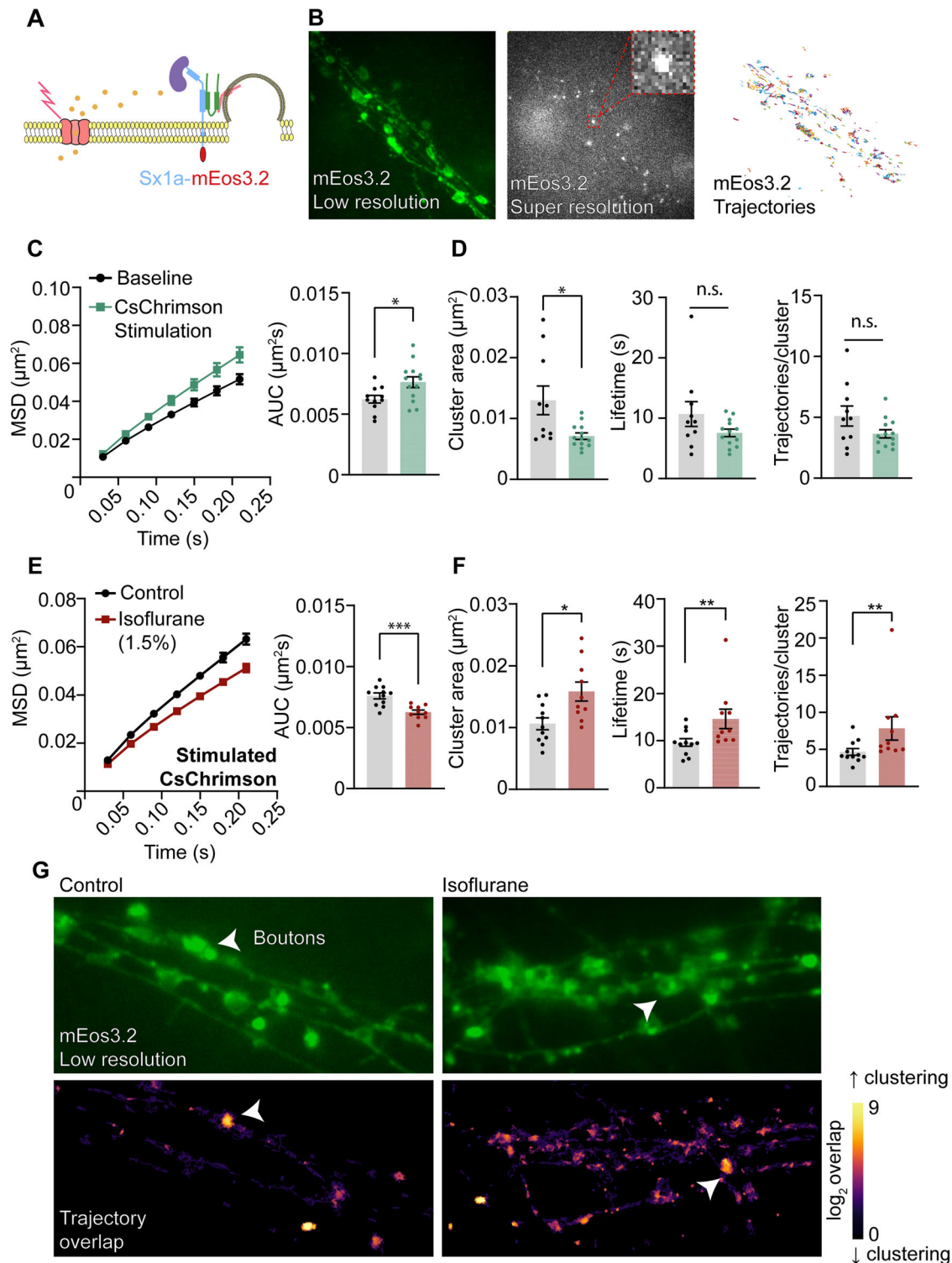
Figure 3. Sx1a mobility dynamics are altered by neuronal Ca^{2+} stimulation and isoflurane anesthesia in cholinergic synapses. **A**, Schematic of the SNARE complex proteins with an mEos3.2 photoconvertible tag attached to the extracellular C-terminus of Sx1a (Sx1a-mEos3.2). **B**, Low-resolution unphotoconverted Sx1a-mEos3.2 in cholinergic synapses (left), super-resolution photo-converted Sx1a-mEos3.2 (middle, highlighted inset of a single molecule), and trajectories from analyzed Sx1a-mEos3.2 molecules. **C**, CsChrimson activation of cholinergic synapses increases the MSD and the AUC of Sx1a-mEos3.2 molecules ($n = 11$ baseline; $n = 13$ stimulated; $p = 0.026$; rank biserial correlation, $r = 0.538$; Mann–Whitney U test; ±SEM). **D**, Sx1a-mEos3.2 were relieved from clusters under CsChrimson activation (left, $p = 0.02$; rank biserial correlation, $r = -0.574$; Mann–Whitney U test) in line with an increase of mobility but did not significantly alter the time spent in clusters (middle, $p = 0.208$; rank biserial correlation, $r = -0.32$; Mann–Whitney U test) or the number of trajectories per cluster (right, $p = 0.203$; rank biserial correlation, $r = -0.323$; Mann–Whitney U test). All data ± SEM. **E**, Isoflurane anesthesia significantly decreased the mobility of Sx1a-mEos3.2 in cholinergic synapses in response to CsChrimson activation ($n = 11$ control; $n = 10$ isoflurane; $p = 0.0008$; rank biserial correlation, $r = -0.818$; Mann–Whitney U test; ±SEM). **F**, Clustering phenotype of Sx1a-mEos3.2 under isoflurane anesthesia was significantly altered. The cluster area (left, $p = 0.022$; rank biserial correlation, $r = 0.6$; Mann–Whitney U test), lifetime (middle, $p = 0.0079$; rank biserial correlation, $r = 0.673$; Mann–Whitney U test), and number of trajectories per cluster (right, $p = 0.0051$; rank biserial correlation, $r = 0.70$; Mann–Whitney U test) all significantly increased during CsChrimson activation and isoflurane anesthesia. All data ± SEM. **G**, Segment overlap plots generated by segNASTIC highlighting increased clustering in the isoflurane condition around boutons (indicated by white arrows).
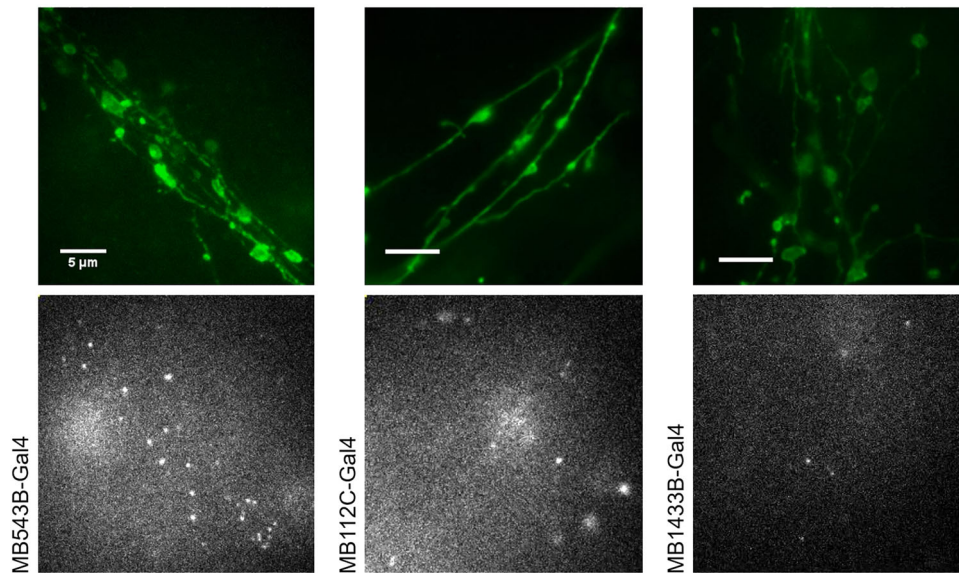
Movie 2. (Associated with Fig. 3). Imaging Sx1a-mEos3.2 single-molecule dynamics from cholinergic, GABAergic, and glutamatergic synapses. Top, Green Sx1a-mEos3.2 images of the three neurotransmitter circuits (acetylcholine, GABA, and glutamate). Bottom, Example recordings of photoconverted single-molecule Sx1a-mEos3.2 activity in the same circuits. [view online]

that showed impaired neurotransmission, we tagged Sx1a with the photoconvertible fluorophore mEos3.2 and generated a transgenic UAS-Sx1a-mEos3.2 fly strain to perform sptPALM in our ex vivo fly brain preparation (Fig. 3A; Movie 2). Our Sx1a-mEos3.2 transgene was reliably expressed within the MB543B-Gal4 cholinergic neurons, allowing us to perform sptPALM of photoconverted molecules within the confines of these cholinergic synapses (Fig. 3B). To stimulate synaptic release, we opted to use a mVenus- instead of the mCherry-tagged CsChrimson channelrhodopsin to avoid spectral overlap with photoconverted mEos3.2 signals. To validate our approach and to understand the effects of stimulation on Sx1a-mEos3.2 dynamics, we first compared the mobility and clustering of Sx1a molecules under stimulated or unstimulated conditions (±ATR; see Materials and Methods, Fly stocks). Upon red-light (561 nm) stimulation, Sx1a-mEos3.2 mobility at cholinergic synapses was significantly increased, as quantified by the MSD and a correspondingly increased AUC (Fig. 3C). This indicates that Ca^{2+} influx-triggered release increases the mobility and diffusion of these molecules (Padmanabhan et al., 2020). To see if the spatiotemporal clustering of Sx1a-mEos3.2 was altered through CsChrimson activation, trajectories were analyzed using the segNASTIC software to see if this correlated with changes in molecule diffusion (Wallis et al., 2023). We revealed that there was a significant decrease in the cluster area of these molecules but no significant changes to the average lifetime of a cluster or the number of trajectories per cluster (Fig. 3D). A similar increase in the mobility of Sx1a has been previously reported in excitatory glutamatergic motor neuron synapses (Bademosi et al., 2017), which could be indicative of the release of Sx1a from presynaptic nanoclusters, binding to other SNARE proteins and the subsequent recruitment to active zones (Ullrich et al., 2015; Padmanabhan et al., 2020).

It has been shown that general anesthetics, both intravenous and volatile, decrease the lateral diffusion of Sx1a on the plasma membrane by trapping them into potentially nonfunctional nanoclusters in fly larval motoneurons as well as heterogeneous adult fly brain neurons (Bademosi et al., 2018b; Hines and van Swinderen, 2021). Consistent with these previous findings, we observed a significant decrease in Sx1a-mEos3.2 mobility in activated cholinergic neurons in the presence of isoflurane (Fig. 3E). We also found a significant increase in the cluster area, lifetime, and the number of Sx1a trajectories per cluster (Fig. 3F). These data indicate that the trapping of Sx1a on the plasma membrane under isoflurane is not a failure of the stimulation, but rather Sx1a becomes compromised in a way that renders the protein trapped and potentially nonfunctional (Fig. 3G).

We sought a different (nonanesthetic) way to impair presynaptic function and see if this also resulted in immobilized and clustered Sx1a-mEos3.2 protein at these cholinergic synapses. We impaired presynaptic function during fly brain development by expressing a tetanus toxin light chain (TeTx-LC) protein in the MB543B cholinergic neurons (Fig. 4A–C). We found that disrupting cholinergic release this way significantly impaired the diffusion of Sx1a molecules (Fig. 4D–F), confining Sx1a predominately into larger and denser clusters (Fig. 4G–I). This suggests that Sx1a clustering might be indicative of decreased or impaired neurotransmission, consistent with the conclusions from our isoflurane experiments.

Sx1a interacts with several other presynaptic proteins to promote the release of neurotransmitters (Sudhof and Rizo, 2011). To determine if other presynaptic proteins might be similarly affected, we next measured the effects of isoflurane on the fly homolog of Munc-18a, which is called Rop (Ras opposite) in *Drosophila*. We selected Rop because it is closely associated with Sx1a before SNARE formation: Munc-18 is responsible for chaperoning Sx1a to the plasma membrane and keeping it in a closed conformation (Kasula et al., 2016) until both interact with other SNARE-associated proteins at active release sites (Harrison et al., 1994; Dulubova, 1999; Rowe et al., 2001). We therefore generated a UAS-Rop-mEos3.2 transgenic fly line and measured the dynamics of Rop-mEos3.2 mobility at the same MBON cholinergic synapses as before (Fig. 5A,B). Like Sx1a, isoflurane decreased Rop-mEos3.2 lateral diffusion during CsChrimson activation, as evidenced by reductions in both the MSD and AUC (Fig. 5C). This was accompanied by a significant increase in the cluster area of Rop proteins but no change in lifetime or trajectories per cluster (Fig. 5D). Unlike Sx1a, isoflurane
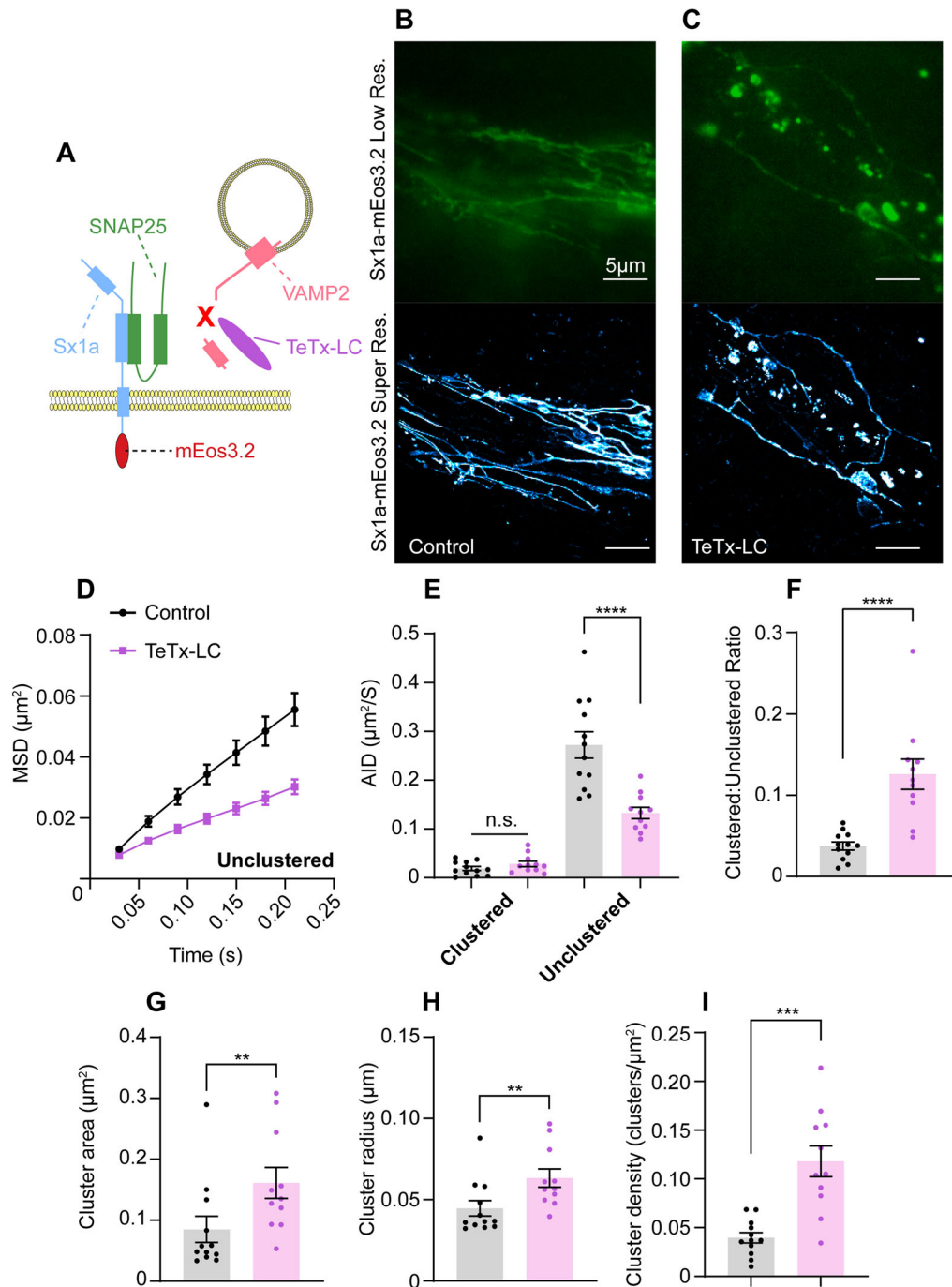
Figure 4. TeTx-LC disruption of cholinergic synapse development impairs Sx1a-mEos3.2 mobility. **A**, Schematic of the SNARE complex with Sx1a-mEos3.2 and TeTx-LC cleavage of VAMP2. **B**, Expression patterns of Sx1a-mEos3.2 within the synapses of the MB543B-Gal4 cholinergic MBON in low resolution (top) and super resolved (bottom) in 3–5-d-old female fruit fly brains (scale bar, 5 μm). **C**, Expression pattern of Sx1a-mEos3.2 as in **B** but with developmental TeTx-LC expression (scale bar, 5 μm). **D**, MSD analysis of Sx1a-mEos3.2 for unclustered trajectories reveals a significant decrease in mobility with TeTx-LC cleavage of VAMP2, resulting from disordered synaptic organization (control, $n = 12$; TeTx-LC, $n = 11$). **E**, The average instantaneous diffusion of both clustered and unclustered Sx1a-mEos3.2 trajectories reveals a significant decrease in diffusion of the unclustered population without affecting the mobility within clusters (clustered control, ns $p = 0.2351$; rank biserial correlation, $r = 0.3$; Mann–Whitney U test; unclustered control, $p = 0.00025$; rank biserial correlation, $r = -0.91$; Mann–Whitney U test). **F**, The number of clustered to unclustered trajectories significantly increased with TeTx-LC ($p = 0.00025$; rank biserial correlation, $r = 0.91$; Mann–Whitney U test). **G–I**, Alongside an increase in cluster number, TeTx-LC also significantly increased the cluster area ($p = 0.009$; rank biserial correlation, $r = 0.636$), radius ($p = 0.009$; rank biserial correlation, $r = 0.636$), and density of Sx1a-mEos3.2 of trajectories in cholinergic synapses ($p = 0.0006$; rank biserial correlation, $r = 0.848$; Mann–Whitney U test). All data ± SEM.

does not cause the trapping of Rop into nanoclusters, presumably because it is still able to disassociate from Sx1a upon reaching an active release site. This suggests that Sx1a/Rop (Sx1a/Munc18) together presents a target for isoflurane before SNARE formation, also potentially revealing that the diffusion and clustering

phenomenon observed may be two separate phenomena. Decreases in diffusion could be due to some interactions with the Sx1a/Rop complex (G. A. Han et al., 2010), whereas clustering of Sx1a could occur postrecruitment to an active zone, without Rop involvement. It is, for example, understood that
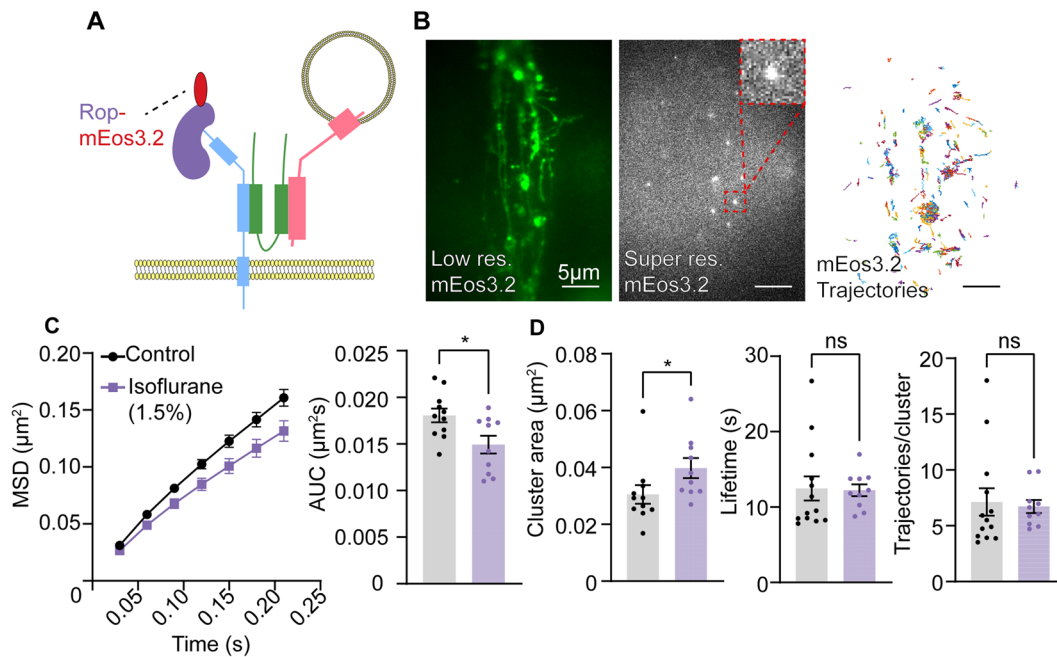
Figure 5. Rop experiences lateral trapping and clustering under isoflurane anesthesia in cholinergic neurons. *A*, Schematic showing the SNARE complex with Rop tagged with an mEos3.2 photoconvertible tag on its C-terminus. *B*, Low-resolution (left), super-resolution photoconverted (middle), and trajectories (right) of Munc18-mEos3.2 molecules in cholinergic synapses using the split MB543B-Gal4. *C*, The MSD and AUC for Munc18-mEos3.2 mobility during CsChrimson activation significantly decreased under isoflurane anesthesia (*n* = 11 control; *n* = 10 isoflurane; *p* = 0.0295; rank biserial correlation, *r* = −0.56; Mann–Whitney *U* test; ±SEM). *D*, In conjunction with a decrease in mobility, Munc18-mEos3.2 molecules experienced a significant increase in the cluster area consistent with Sx1a-mEos3.2 (*p* = 0.01; rank biserial correlation, *r* = 0.7; Mann–Whitney *U* test; ±SEM).

Munc18a chaperones Sx1a to the plasma membrane, before both proteins terminate their journey to active zones (Kasula et al., 2016; Arnold et al., 2017; Lai et al., 2017; Shu et al., 2019; Yang et al., 2022).

Having found that isoflurane affects the mobility of Sx1a and Rop at presynapses, we wondered whether the same effects could be observed for Sx1a localized in extrasynaptic compartments (Fig. 6A; Ribrault et al., 2011; Maidorn et al., 2019). Interestingly, during CsChrimson activation, extrasynaptic Sx1a also displayed a significant decrease in lateral diffusion under isoflurane anesthesia, as measured by the MSD and AUC (Fig. 6B). However, in contrast to Sx1a localized to the synapse, there was no clustering phenotype under isoflurane observed in extrasynaptic regions (Fig. 6C). This suggests that while lateral trapping of Sx1a (or Rop) seems to be a common feature of general anesthesia (Bademosi et al., 2018b; Hines and van Swinderen, 2021), the nanoclustering phenotype may be dependent on other Sx1a-interacting proteins at presynaptic active zones (Fig. 6D).

Sx1a dynamics and neurotransmission in GABAergic and glutamatergic neurons are mostly unaffected by isoflurane

Recent mammalian studies suggest that general anesthetics do not target all neurotransmitter systems equally (Zimin et al., 2016, 2018; Koyanagi et al., 2019; Zhou et al., 2019; Speigel et al., 2022). A possible explanation for this is that the distribution of SNARE protein isoforms is not unilateral across neurotransmitter subtypes (Benagiano et al., 2011). We therefore selected split-Gal4 MBONs that specifically express GABA or glutamate (Fig. 7A,D), to examine whether Sx1a mobility was also impacted by isoflurane in these different neurons (MB112C-Gal4 and MB433B-Gal4, respectively; Aso et al., 2014). While GABA is inhibitory in the adult *Drosophila* brain,

the role of glutamate in the adult fly brain remains ambiguous, and glutamate has been shown to exert inhibitory functions in the adult CNS (Chvilicek et al., 2020; Vrontou et al., 2021), whereas it is known to be excitatory at the neuromuscular junction (Jan and Jan, 1976; Liu and Wilson, 2013; Molina-Obando et al., 2019). We expressed Sx1a-mEos3.2 in either set of neurons and found that we were able to track Sx1a dynamics reliably (Fig. 7B,E; Movie 2). We followed the exact same optogenetic excitation protocol as for the cholinergic neurons (see Materials and Methods). We observed no significant decrease in mobility and no increase in clustering for Sx1a molecules in isoflurane-exposed brains compared with those in controls, for both GABAergic and glutamatergic synapses (Fig. 7C,F). This suggests a level of resistance to isoflurane in the vesicle release machinery characteristic of inhibitory presynapses.

We therefore questioned whether neurotransmission from GABAergic and glutamatergic neurons was also insensitive to isoflurane. To test this, we performed synaptopHluorin imaging in these neurons (Fig. 8A,D). For both GABA and glutamate, no significant difference was observed for the total relative fluorescence, activity, or ROI density of synaptopHluorin release in the presence of isoflurane when compared with control (Fig. 8B,E). When we then compared different release size groups, isoflurane did not change the release characteristics of the different ROIs; however, there was a significant decrease in the relative frequency of the small release group for glutamate (Fig. 8C,F). We noted that synaptopHluorin results were also more variable in these neurons, so it is possible that these include a subset of synapses (e.g., smaller glutamatergic ones) that are impacted by isoflurane. Compared with the cholinergic neurons, the larger ROIs contributed more to the total relative activity in GABAergic and glutamatergic neurons (Fig. 8G,H). Since a larger proportion of release from cholinergic synapses was from small-
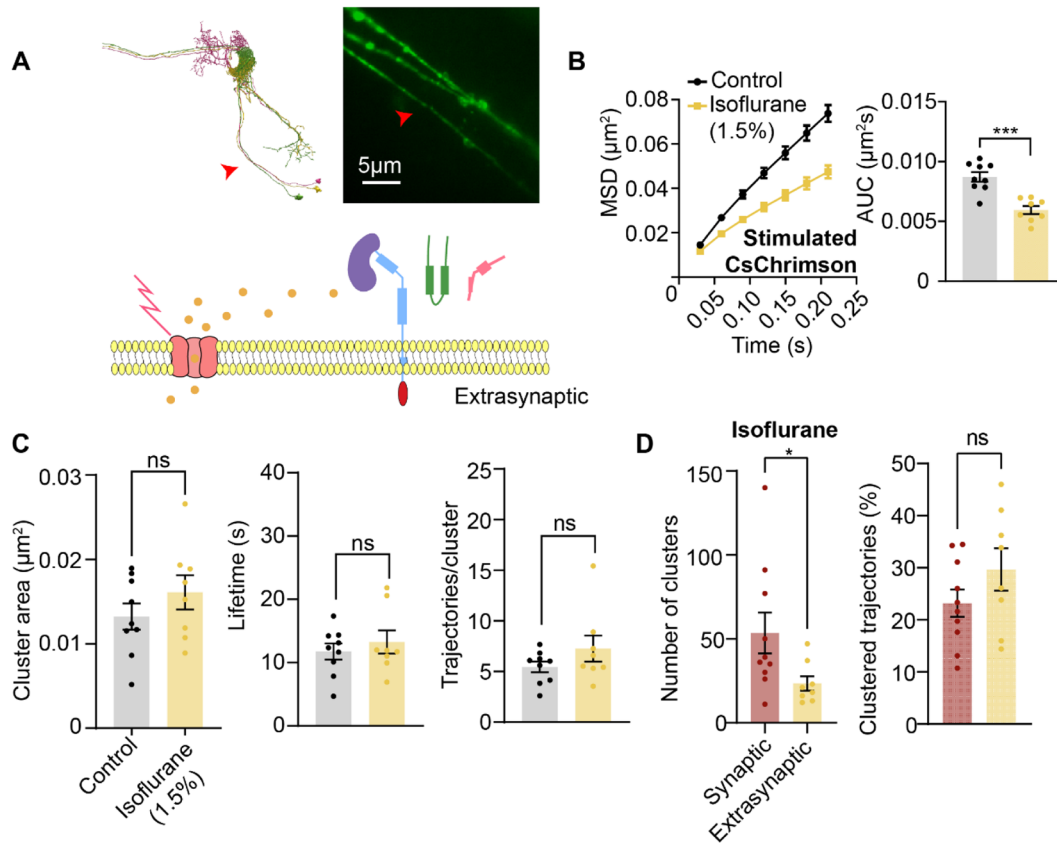
Figure 6. Isoflurane fails to cluster Sx1a in extrasynaptic compartments of cholinergic neurons. *A*, Neural skeleton of MB543B-Gal4 derived from FIB-SEM *Drosophila* brain volume (left) with a close-up of the extrasynapses expressing Sx1a-mEos3.2 (right). Red arrow indicates the area of the close-up. *B*, Isoflurane anesthesia is able to significantly restrict CsChrimson-activated Sx1a-mEos3.2 mobility in the absence of synaptic architecture by decreasing the MSD and AUC ($n = 9$ control; $n = 8$ isoflurane; $p = 0.0006$; rank biserial correlation, $r = -0.92$; Mann–Whitney U test; ±SEM). *C*, Compared to the synaptic compartment, isoflurane was unable to alter the clustering dynamics of Sx1a-mEos3.2 in the extrasynapse. No significant change in the cluster area (left, $p = 0.37$; rank biserial correlation, $r = 0.28$; Mann–Whitney U test), lifetime (middle, $p > 0.999$; rank biserial correlation, $r = 0$; Mann–Whitney U test), or number of trajectories per cluster (right, $p = 0.541$; rank biserial correlation, $r = 0.194$; Mann–Whitney U test) was observed. All data ± SEM. *D*, Comparison between the number of clusters in the presence of isoflurane between synaptic and extrasynaptic compartments was significantly lower for extrasynapses ($p = 0.043$; rank biserial correlation, $r = -0.575$; Mann–Whitney U test); however, a number of trajectories that were clustered between the two were not significantly different ($p = 0.203$; rank biserial correlation, $r = 0.375$; Mann–Whitney U test). All data ± SEM.

and medium-sized ROIs, resistance to the overall decreased transmitter release in inhibitory synapses could be due to the comparatively lower activity in smaller ROIs (Fig. 8*G*,*H*). Taken together, our neurotransmission results are nevertheless consistent with our Sx1a imaging results: isoflurane impairs presynaptic function in cholinergic synapses, but not in GABAergic synapses and less so in glutamatergic synapses—at least in these adult MBONs.

Synapse-specific effects are not caused by differential calcium influx
We considered an alternative explanation for the differential presynaptic effects we found among the three MBONs: changes in the apparent level of exocytosis under isoflurane may simply reflect decreased excitability of the neurons in question. In other words, the same optogenetic stimulation may produce lower excitability in some circuits compared with others and therefore result in reduced correlates of exocytosis. Indeed, there is in vitro evidence for general anesthetics impairing the function of presynaptic calcium channels (Baumgart et al., 2015; Koyanagi et al., 2019), which if differentially expressed could explain our results. To test this possibility, we exchanged UAS-synaptopHluorin for UAS-GCaMP6s, which we have used previously to measure neural excitability by tracking calcium influx

into the cell (Troup et al., 2023). We followed the same CsChrimson-mediated stimulation protocol to ensure that our GCaMP6s data were comparable with the synaptopHluorin and Sx1a-mEos3.2 data (see Materials and Methods), and we focused on the excitatory cholinergic circuit (MB543B) and the inhibitory GABAergic circuit (MB112C). We first confirmed that GCaMP6s was expressed in either MBON (Fig. 9*A*,*E*) and that our red-light regime produced a calcium transient across both circuits (Fig. 9*C*,*G*, black line; Movie 3). Interestingly, isoflurane exposure did not significantly affect calcium transients in both the cholinergic and GABAergic MBONs (Fig. 9*C*,*G*; cholinergic, red line; GABAergic, purple line). While it is possible that the neurons have different baseline activity levels (this could not be addressed in our paradigm), it seems that isoflurane has no effect on induced activity.

We wondered whether distinct effects on calcium transients could be uncovered by disambiguating neural compartments of different sizes. We have shown previously that exocytosis from smaller ROIs was more susceptible to the effects of isoflurane and contributed disproportionally to the overall effect (Fig. 2). We therefore segregated our GCaMP6s data into small, medium, and large ROIs (Fig. 9*B*,*F*), following the same logic as before. We did not detect any significant effects of isoflurane across any ROI size category, for either the cholinergic or the GABAergic circuit
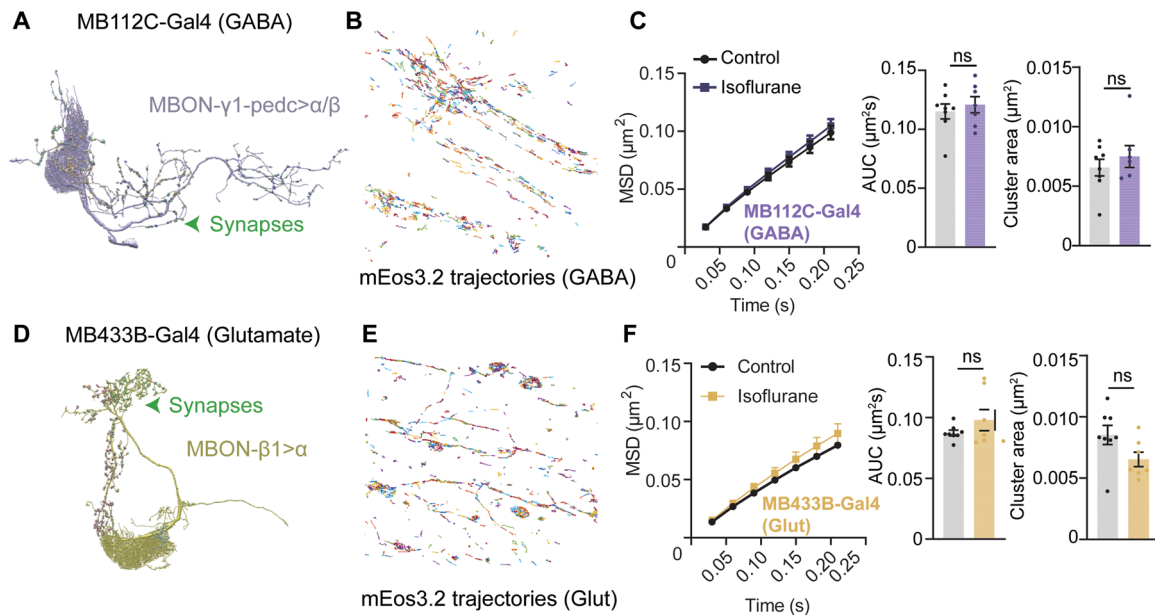
Figure 7. Sx1a dynamics are unaffected by isoflurane in GABAergic and glutamatergic MBONs. **A**, A GABAergic MBON driven by MB112C-Gal4, with imaging, is indicated (synapses). **B**, Sx1a-mEos3.2 trajectories for MB112C-Gal4 (GABA) inhibitory synapses. **C**, Sx1a-mEos3.2 MSD, AUC, and the cluster area are unaffected by isoflurane anesthesia in GABA synapses ($n = 8$ control; $n = 7$ isoflurane; AUC, $p = 0.728$; rank biserial correlation, $r = 0.125$; cluster area, $p = 0.867$; rank biserial correlation, $r = 0.071$; Mann–Whitney U test). All data $\pm$ SEM. **D**, A glutamatergic MBON driven by MB433B-Gal4, with imaging, is indicated (synapses). **E**, Sx1a-mEos3.2 trajectories for MB433B-Gal4 (Glut) inhibitory synapses. **F**, Sx1a-mEos3.2 MSD, AUC, and the cluster area are unaffected by isoflurane anesthesia in glutamatergic inhibitory synapses ($n = 8$ control; $n = 7$ isoflurane; AUC, $p = 0.955$; rank biserial correlation, $r = 0.036$; cluster area, $p = 0.054$; rank biserial correlation, $r = -0.607$; Mann–Whitney U test). All data $\pm$ SEM.

(Fig. 9D,H; cholinergic, red lines; GABAergic, purple line), although a similar trend toward lower calcium was noted across all ROIs. This suggests that the differential effects of isoflurane that we observed for our exocytosis readouts are unlikely to be due to differences in excitability in these specific neurons.

Discussion

Over the last few decades, several targets of general anesthetics in the CNS have emerged to potentially explain their unique ability to produce a rapid loss of consciousness and unresponsiveness (Franks, 2008; Hemmings et al., 2019). Explanations for general anesthesia have largely focused on mechanisms that reduce neuronal excitability through postsynaptic potentiation of inhibitory receptors such as GABA$_A$ (Franks and Lieb, 1984, 1994; Tomlin et al., 1998). Recently, a complementary set of potential mechanisms have begun to emerge by examining presynaptic disruptions in neurotransmission (Ouyang et al., 2003; Hemmings et al., 2005, 2019; Franks, 2008; Herring et al., 2009, 2011; Xie et al., 2013; van Swinderen and Kottler, 2014; Baumgart et al., 2015; Zimin et al., 2018; Koyanagi et al., 2019; Torturo et al., 2019; Zhou et al., 2019; Speigel and Hemmings, 2021; Jung et al., 2022). However, it remains unclear which of the presynaptic processes are most relevant and in which neurons specifically. Our study uncovers unequal effects of isoflurane on different neurotransmitter systems in the *Drosophila* brain, defined by whether they are excitatory or inhibitory. This supports recent work in rodent models that also uncovered unequal effects of isoflurane at excitatory and inhibitory synapses (Zimin et al., 2016, 2018; Speigel et al., 2022). While our study only examined specific MBONs in the adult *Drosophila* brain, future experiments should determine whether our findings generalize to other neurons in the fly model and whether these are indeed grouped by neurotransmitter type.

There are several explanations for why excitatory synapses might present distinct target for general anesthetics. It has been suggested that differences in the expression of voltage-gated sodium and/or calcium channels could be responsible for the differential sensitivity to isoflurane in different neuronal subtypes (Baumgart et al., 2015; Torturo et al., 2019; Speigel and Hemmings, 2021). Our results suggest that the role of these presynaptic cation channels might not be directly relevant, at least in the *Drosophila* MBONs examined, because we expect that Ca^{2+} entry induced by the activation of CsChrimson is comparable in all three circuits tested and would also be "downstream" of any sodium channel effects. Indeed, imaging GCaMP6s revealed calcium transients in activated cholinergic and GABAergic MBONs, which were not significantly affected by isoflurane exposure (Fig. 9). We can therefore conclude that the significant effects we observed on neurotransmission as well as the diffusion and clustering of Sx1a could be independent of Ca^{2+} channel activity or overall MBON excitability. This provides support to the view that general anesthetics such as isoflurane and propofol also act downstream from presynaptic channels (Wang et al., 2020) by interacting directly with SNARE molecules (Nagele et al., 2005; Bademosi et al., 2018b; Hines and van Swinderen, 2021). However, it remains likely that diverse presynaptic targets work synergistically to impair neurotransmission (Hemmings et al., 2019). For example, several general anesthetics have been shown to affect mitochondrial function (Morgan et al., 2002; Perouansky et al., 2023), so distinct metabolic requirements across neural subtypes could differentially affect neurotransmitter release and recycling dynamics at excitatory versus inhibitory synapses (Jung et al., 2022). All of our experiments were done in physiological HL3.1 solution which has high sucrose levels (Feng et al., 2004). This may have masked any metabolic distinctions among the neural subtypes or synaptic compartments but by the same token exposed the SNARE-related differences that we found.
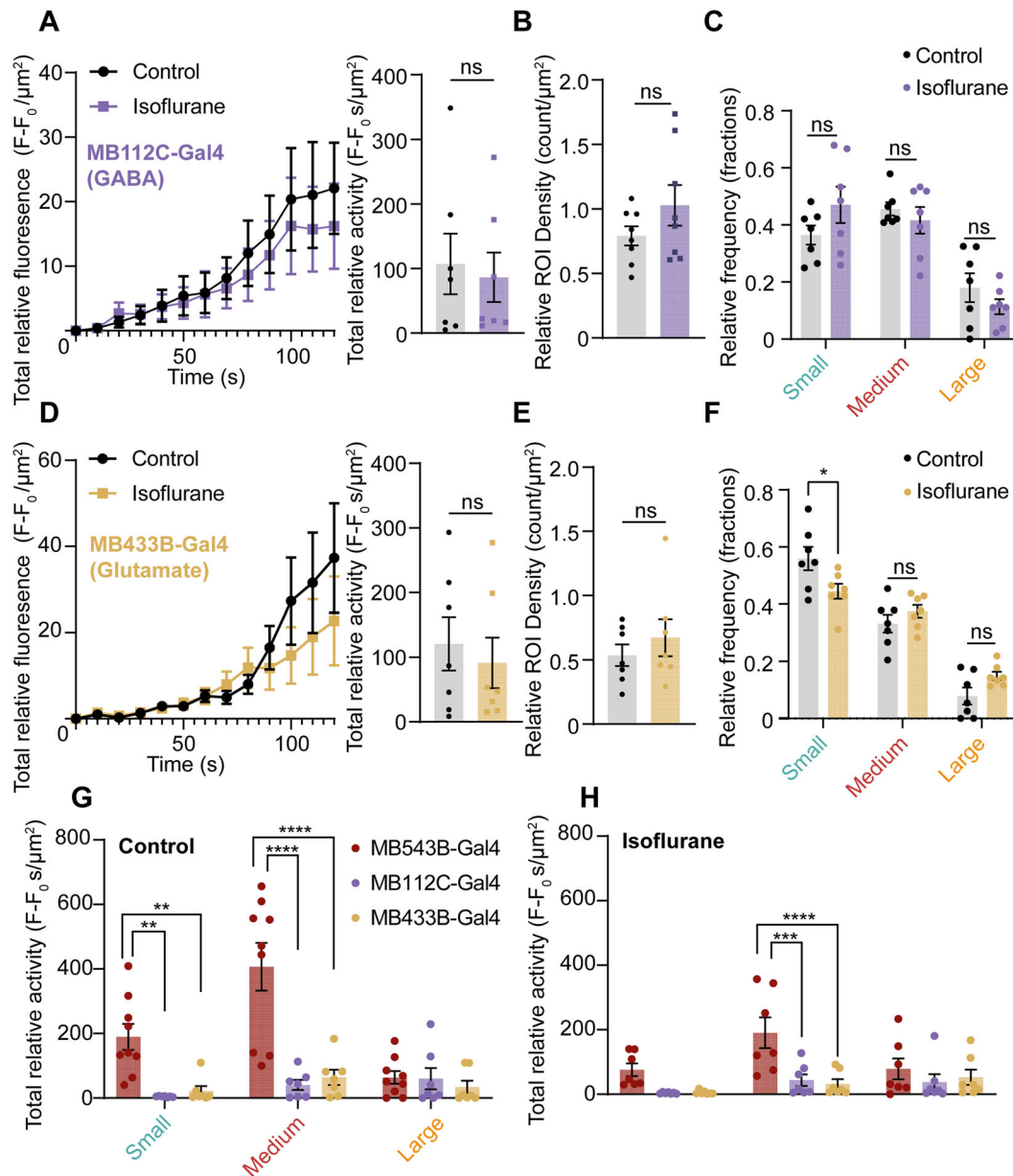
Figure 8. Synaptic release in GABAergic and glutamatergic MBONs is unaffected by isoflurane. **A**, Total relative fluorescence and activity from GABAergic synapses is unaffected by isoflurane ($n = 7$ control and isoflurane; $p = 0.901$; rank biserial correlation, $r = 0.06$; Mann–Whitney U test). All data ± SEM. **B**, The relative ROI density was unaffected by isoflurane in GABA synapses ($p = 0.44$; rank biserial correlation, $r = 0.25$; Mann–Whitney U test; ±SEM). **C**, Isoflurane anesthesia's impact on the relative distribution of ROI sizes was assessed across small, medium, and large groups, revealing no significant differences (small group, $F_{(1,12)} = 0.011$; $p = 0.918$; medium group, $F_{(1,12)} = 1.500$; $p = 0.244$; large group, $F_{(1,12)} = 0.883$; $p = 0.366$; ANOVA). All data ± SEM. **D**, Like GABA synapses, release from glutamatergic synapses is also unaffected by isoflurane anesthesia ($n = 7$ control and isoflurane; $p = 0.71$; rank biserial correlation, $r = -0.14$; Mann–Whitney U test). All data ± SEM. **E**, Relative ROI density unaffected by isoflurane in glutamatergic synapses ($p = 0.53$; rank biserial correlation, $r = 0.224$; Mann–Whitney U test; ±SEM). **F**, Small ROIs significantly decreased under isoflurane ($F_{(1,14)} = 5.515$; $p = 0.037$; ANOVA), with no difference in release per region size across all sizes (medium, $F_{(1,14)} = 1.259$; $p = 0.284$; large, $F_{(1,14)} = 4.665$; $p = 0.052$; ANOVA). All data ± SEM. **G**, Comparison of total relative activities for the control condition between small, medium, and large for the three neurotransmitter circuits. MB543B-Gal4 had significantly higher activity from small and medium ROIs than MB112C-Gal4 and MB433B-Gal4 ($F_{(2,27)} = 14.35$; $p = 0.0018$; and $F_{(2,27)} = 39.83$; $p = 2.4 \times 10^{-7}$; ANOVA). In contrast, the large ROIs showed no significant difference ($F_{(1,18)} = 0.88$; $p = 0.366$; ANOVA). **H**, Same comparison as **G** but for the isoflurane condition. Only the medium release group for MB543B-Gal4 was significantly higher than MB112C-Gal4 or MB433B-Gal4 ($F_{(2,12)} = 5.48$; $p = 0.017$; $F_{(2,12)} = 4.34$; $p = 0.01$; ANOVA).

While we found no significant effect of isoflurane on MBON excitability (as measured by GCaMP6s activity) in this study, in a previous pan-neuronal, whole-brain imaging study, we did detect a small but significant decrease in the calcium readout (Troup et al., 2023). Importantly, in that previous study, we concluded that isoflurane anesthesia was associated with neural ensemble fragmentation rather than decreased neural activity. This is consistent with our current study finding circuit-specific presynaptic effects rather than general effects on neural excitability. Downscaling of synaptic release from subpopulations of excitatory neurons could lead to ensemble fragmentation, without significantly affecting overall neural excitability.

How isoflurane-mediated Sx1a lateral trapping and clustering might cause decreased neurotransmission in the cholinergic neurons remains unclear, particularly since the precise location of clustering relative to active release sites is unknown. A previous
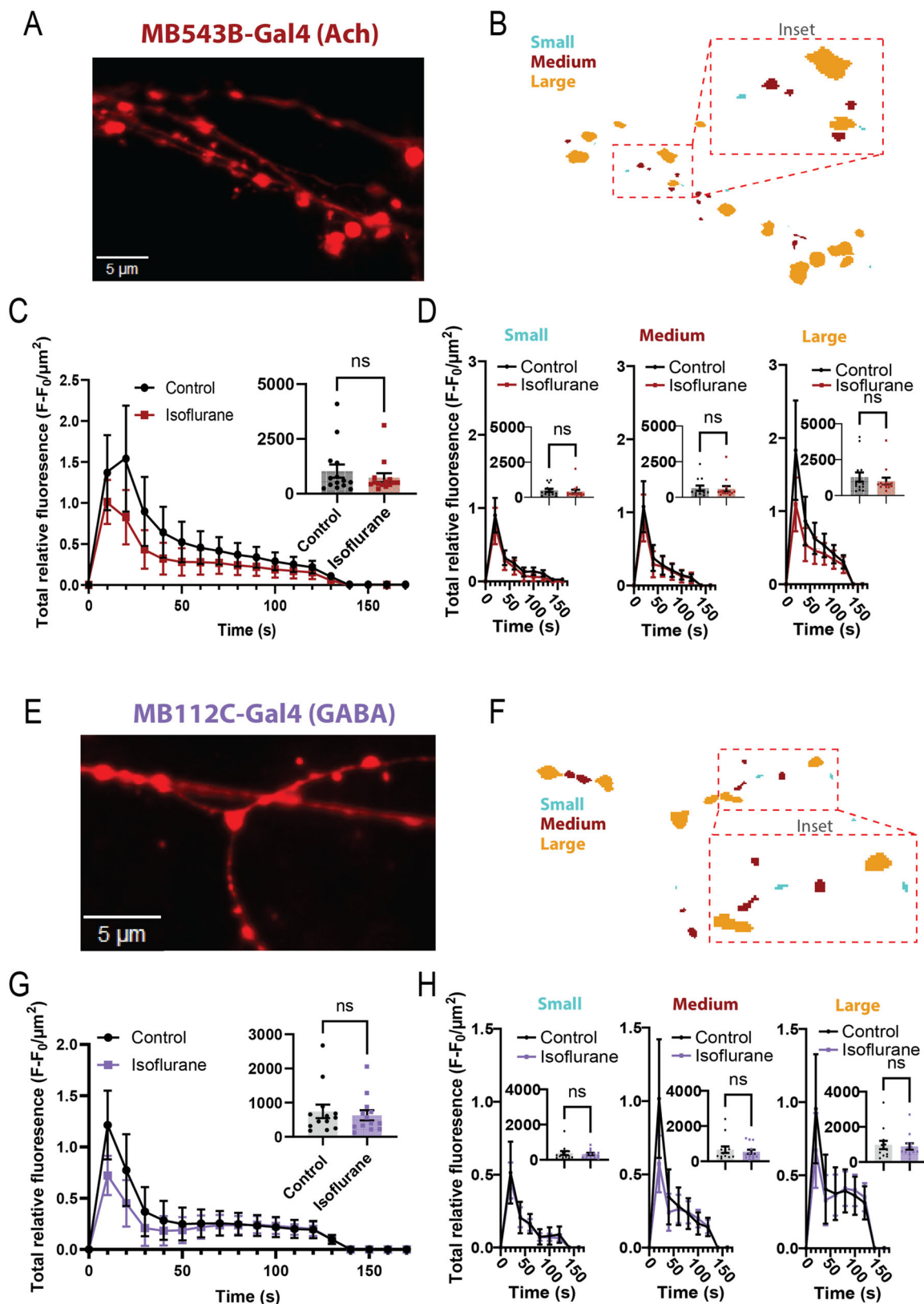
Figure 9. Intracellular calcium activity is not significantly affected by isoflurane. **A**, Synaptic domain of cholinergic MB543B-Gal4, as revealed by CsChrimson-linked mCherry (scale bar, 5 μm). **B**, Separation of GCaMP6s activity in the same MB543-Gal4 neuron as in **A** into small (<0.08 μm^2), medium (0.09–0.42 μm^2), and large (>0.43 μm^2) ROIs. Inset, an example region with three different ROI categories. **C**, Average GCaMP6s fluorescence traces (±SEM) normalized to the baseline for the control (black) and isoflurane (red) conditions. Inset, average total activity for the control and isoflurane ($n = 14$ control; $n = 14$ isoflurane; $p = 0.66$; rank biserial correlation, $r = -0.1$; Mann–Whitney U test). **D**, Average GCaMP6s fluorescence traces (±SEM) for small (left), medium (middle), and large (right) ROIs. Inset, average total activity for each ROI category (ns, not significant; Mann–Whitney U test). **E–H**, As with **A–D**, for the GABAergic MB112C-Gal4 driver line ($n = 14$ control; $n = 14$ isoflurane; $p = 0.918$; rank biserial correlation, $r = -0.03$; Mann–Whitney U test).

study focusing on the intravenous anesthetic propofol proposed that Sx1a molecules are trapped by the drug into nonfunctional nanoclusters on the plasma membrane, prior to SNARE formation at the active zone (Bademosi et al., 2018b). From our results we can conclude that while lateral diffusion for Sx1a decreases in both extrasynaptic and synaptic compartments, clustering only occurs at synapses (Figs. 3E,F, 6B–D). This indicates that synaptic release architecture must likely be present for Sx1a molecules to cluster under isoflurane anesthesia and that increased clustering potentially occurs after Sx1a recruitment to active zones (Fig. 3G). This conclusion is consistent with the apparent decrease in lateral diffusion and increased clustering of Rop (Munc18; Fig. 5C,D), likely due to its strong interaction with Sx1a immediately prior to SNARE formation (Burkhardt et al., 2008).

Why might neurotransmission be more vulnerable to isoflurane in excitatory neurons? One explanation is likely to be metabolic (Zimin et al., 2016, 2018), although this could also depend on the stimulation regime and associated neurotransmitter recycling dynamics (Jung et al., 2022). We employed the same stimulation regime in HL3.1 solution (which is high in sugar content;

Movie 3. (Associated with Fig. 9). Imaging GCaMP6s in CsChrimson-activated cholinergic and GABAergic circuits. Left, Activated MB543B-Gal4 (cholinergic). Right, Activated MB112C-Gal4 (GABAergic). [view online]

Feng et al., 2004) in all of our experiments, suggesting a different explanation more closely linked to the exocytosis machinery rather than metabolic constraints. Although the synaptic release machinery is extremely conserved (Sudhof and Rizo, 2011), different neurons can express distinct SNARE isoforms (Ruiz-Montasell et al., 1996; Augustin et al., 1999; Kádková et al., 2019), for example, SNAP25, which has been shown to be absent in some inhibitory neurons (Su et al., 2001; Verderio et al., 2004; Frassoni et al., 2005; Holt et al., 2006; Garbelli et al., 2008; Mandolesi et al., 2009). Given that we saw a clear isoflurane phenotype in the excitatory cholinergic system and no effect in the inhibitory GABAergic and glutamatergic circuits, it is reasonable to hypothesize that the latter neurons could express different variants of the exocytotic machinery. Future experiments aimed at explaining our findings might focus on investigating whether anesthesia-resistant neurons might be grouped by their presynaptic machinery components rather than by the specific neurotransmitter that is released. While glutamatergic synapses are excitatory in the adult mouse brain (and affected by general anesthetics; Baumgart et al., 2015; Zimin et al., 2016, 2018), they can be inhibitory in the adult fly brain (Liu and Wilson, 2013), so they could comprise distinct presynaptic target mechanisms. Glutamate can also be excitatory in *Drosophila*, for example, in larval motoneurons (Xue and Zhang, 2002), and interestingly larval glutamatergic synapses are impaired by both isoflurane (Zalucki et al., 2015) and propofol (Karunanithi et al., 2020). The fact that general anesthetics impair release from excitatory cholinergic MBONs (this study) as well as excitatory glutamatergic larval motoneurons (Zalucki et al., 2015; Karunanithi et al., 2020) argues for a generalizable presynaptic effect linked to their excitatory quality rather than a neurotransmitter subtype.

Another interesting observation from our study that aligns well with observations from larval motoneurons (Karunanithi et al., 2020) is that larger release sites seem resistant to general anesthetics (Fig. 2D). Among the three neurotransmitter systems that we tested, the distribution of synaptopHluorin ROI sizes
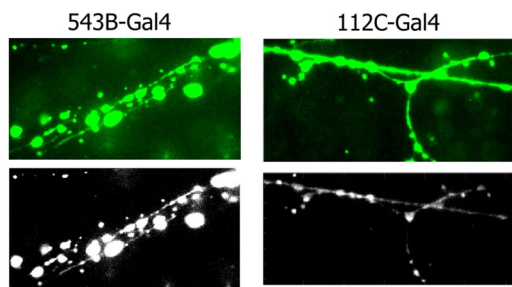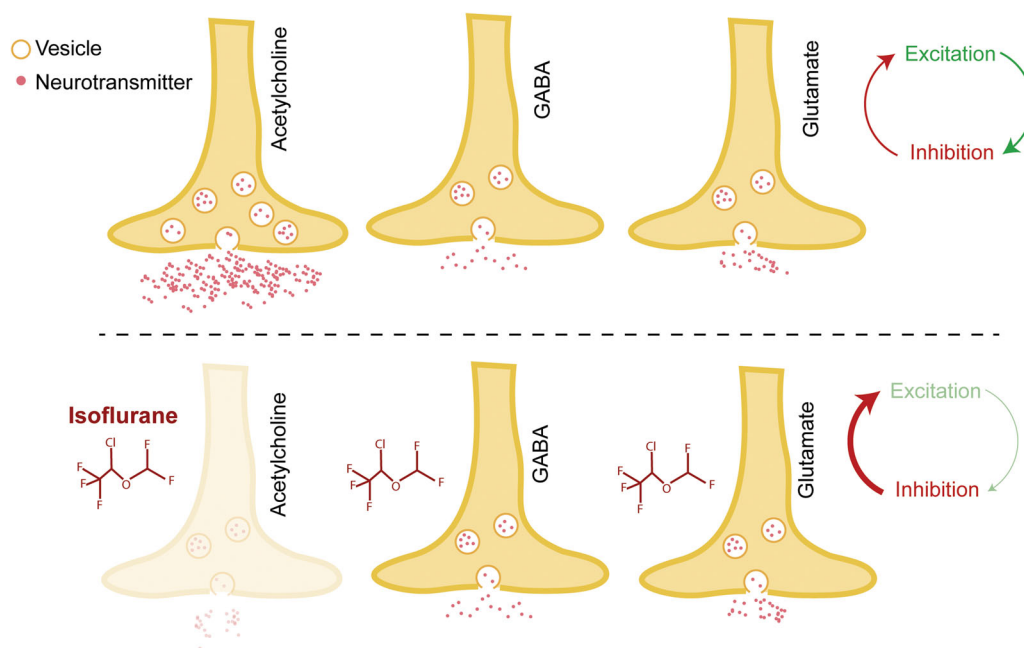
Figure 10. Schematic of the presynaptic effect of isoflurane on three MBONs. In the presence of isoflurane, excitatory cholinergic neurotransmitter release is impaired, while glutamatergic and GABAergic release is unaffected. Decreased excitation and sustained inhibition coupled to potentiation of postsynaptic GABA receptors would lead to successive bouts of inhibition in the brain.

between them did not change much; however, the relative contribution of each size group to the overall activity skewed toward larger ROIs in inhibitory MBONs (Fig. 8G,H). This is likely related to the way some inhibitory synapses develop, typically less efficient at vesicle recycling and driven by more tonic release mechanisms (Häusser and Clark, 1997; Bae et al., 2020). Studies have shown a correlation between the size and release capacity of an active zone and the number of tethered vesicles by SNARE molecules localized to them, which could provide resistance to the effects of general anesthetics due to the greater amount of release architecture present (J. Han et al., 2017), as well as greater metabolic support (Jung et al., 2022). However, synaptopHluorin ROI size alone could not fully account for differences between neurotransmitter groups as there was no direct effect on the diffusion dynamics of Sx1a molecules in inhibitory synapses (Fig. 7). These findings indicate dual mechanisms that are based on presynaptic targeting of excitatory neurons by severely disrupting smaller and more active release sites with specific targeting of Sx1a molecules and cognate SNARE partners (including Munc18; Fig. 5), which have previously been reported to be binding targets of several general anesthetics (Nagele et al., 2005; Xie et al., 2013; Woll et al., 2016).

From our findings, it is evident that neurons in the fly CNS are differentially affected by general anesthetics, with clear differences between MBONs expressing different neurotransmitter subtypes (Fig. 10). Our findings align well with other studies in mammals where excitatory neurons show decreased neurotransmission in response to isoflurane anesthesia (Zimin et al., 2016; Koyanagi et al., 2019; Torturo et al., 2019; Speigel and Hemmings, 2021). However, the same studies also provide counterexamples where some excitatory neurons are not affected by isoflurane (Zimin et al., 2016), while some inhibitory neurons are (Speigel and Hemmings, 2021). This suggests a presynaptic explanation independent of the specific neurotransmitter involved, which we propose could be different vesicle release dynamics or architectures (van Swinderen and Kottler, 2014). Considering our findings together with postsynaptic theories, we propose that the brain under general anesthesia could be experiencing synergistic pre- and postsynaptic bouts of inhibition to cause a loss of consciousness and responsiveness: first a circuit-specific inhibition of excitatory activity by effects on postsynaptic receptors embedded in arousal systems (leading to loss of consciousness), accentuated by a more global downscaling of presynaptic release from mostly excitatory neurons. The relative contribution to different anesthesia endpoints as well as recovery dynamics should be discernible in behaving animals (Cylinder et al., 2024), using neuron-specific expression systems as described in this study. Genetic control of distinct SNARE protein isoforms in these specific neural circuits should help uncover the presynaptic mechanisms involved.

References

Arnold MG, Adhikari P, Kang B, Xu H (2017) Munc18a clusters SNARE-bearing liposomes prior to trans-SNARE zippering. Biochem J 474:3339–3354.

Aso Y, et al. (2014) The neuronal architecture of the mushroom body provides a logic for associative learning. Elife 3:e04577.

Augustin I, Betz A, Herrmann C, Jo T, Brose N (1999) Differential expression of two novel Munc13 proteins in rat brain. Biochem J 337:363–371.

Bademosi AT, Lauwers E, Amor R, Verstreken P, van Swinderen B, Meunier FA (2018a) In vivo single-molecule tracking at the Drosophila presynaptic motor nerve terminal. J Vis Exp 131:56952.

Bademosi AT, et al. (2018b) Trapping of syntaxin1a in presynaptic nanoclusters by a clinically relevant general anaesthetic. Cell Rep 22:427–440.

Bademosi AT, Lauwers E, Padmanabhan P, Odierna L, Chai YJ, Papadopulos A, Goodhill GJ, Verstreken P, van Swinderen B, Meunier FA (2017) In vivo single-molecule imaging of syntaxin1A reveals polyphosphoinositide- and activity-dependent trapping in presynaptic nanoclusters. Nat Commun 8:13660–13660.

Bae JR, Lee W, Jo YO, Han S, Koh S, Song WK, Kim SH (2020) Distinct synaptic vesicle recycling in inhibitory nerve terminals is coordinated by SV2A. Prog Neurobiol 194:101879.

Baumgart JP, Zhou Z-Y, Hara M, Cook DC, Hoppa MB, Ryan TA, Hemmings HC (2015) Isoflurane inhibits synaptic vesicle exocytosis through reduced Ca2+influx, not Ca2+ -exocytosis coupling. Proc Natl Acad Sci U S A 112:11959–11964.

Benagiano V, Lorusso L, Flace P, Girolamo F, Rizzi A, Bosco L, Cagiano R, Nico B, Ribatti D, Ambrosi G (2011) VAMP-2, SNAP-25A/B and syntaxin-1 in glutamatergic and GABAergic synapses of the rat cerebellar cortex. BMC Neurosci 12:118.

Bensel BM, Guzik-Lendrum S, Masucci EM, Woll KA, Eckenhoff RG, Gilbert SP (2017) Common general anesthetic propofol impairs kinesin processivity. Proc Natl Acad Sci U S A 114:E4281–E4287.

Bertaccini EJ, Dickinson R, Trudell JR, Franks NP (2014) Molecular modeling of a tandem two pore domain potassium channel reveals a putative binding site for general anesthetics. ACS Chem Neurosci 5:1246–1252.

Burkhardt P, Hattendorf DA, Weis WI, Fasshauer D (2008) Munc18a controls SNARE assembly through its interaction with the syntaxin N-peptide. EMBO J 27:923–933.

Chvilicek MM, Titos I, Rothenfluh A (2020) The neurotransmitters involved in Drosophila alcohol-induced behaviors. Front Behav Neurosci 14:607700.

Cylinder DM, van Zundert AAJ, Solt K, van Swinderen B (2024) Time to wake up! The ongoing search for general anesthetic reversal agents. Anesthesiology 140:610–627.

Dulubova I (1999) A conformational switch in syntaxin during exocytosis: role of munc18. EMBO J 18:4372–4382.

Feng Y, Ueda A, Wu CF (2004) A modified minimal hemolymph-like solution, HL3.1, for physiological recordings at the neuromuscular junctions of normal and mutant Drosophila larvae. J Neurogenet 18:377–402.

Franks NP (2008) General anaesthesia: from molecular targets to neuronal pathways of sleep and arousal. Nat Rev Neurosci 9:370–386.

Franks NP, Lieb WR (1984) Do general anaesthetics act by competitive binding to specific receptors? Nature 310:599–601.

Franks NP, Lieb WR (1994) Molecular and cellular mechanisms of general anaesthesia. Nature 367:607–614.

Frassoni C, Inverardi F, Coco S, Ortino B, Grumelli C, Pozzi D, Verderio C, Matteoli M (2005) Analysis of SNAP-25 immunoreactivity in hippocampal inhibitory neurons during development in culture and in situ. Neuroscience 131:813–823.

Garbelli R, Inverardi F, Medici V, Amadeo A, Verderio C, Matteoli M, Frassoni C (2008) Heterogeneous expression of SNAP-25 in rat and human brain. J Comp Neurol 506:373–386.

Gu H, O'Dowd D (2006) Cholinergic synaptic transmission in adult Drosophila Kenyon cells in situ. J Neurosci 26:265–272.

Han GA, Malintan NT, Collins BM, Meunier FA, Sugita S (2010) Munc18-1 as a key regulator of neurosecretion. J Neurochem 115:1–10.

Han J, Pluhackova K, Böckmann RA (2017) The multifaceted role of SNARE proteins in membrane fusion. Front Physiol 8:5.

Harrison SD, Broadie K, van de Goor J, Rubin GM (1994) Mutations in the Drosophila Rop gene suggest a function in general secretion and synaptic transmission. Neuron 13:555–566.

Häusser M, Clark BA (1997) Tonic synaptic inhibition modulates neuronal output pattern and spatiotemporal synaptic integration. Neuron 19:665–678.

Hemmings HC, Riegelhaupt PM, Kelz MB, Solt K, Eckenhoff RG, Orser BA, Goldstein PA (2019) Towards a comprehensive understanding of anesthetic mechanisms of action: a decade of discovery. Trends Pharmacol Sci 40:464–481.

Hemmings HC, Yan W, Westphalen RI, Ryan TA (2005) The general anesthetic isoflurane depresses synaptic vesicle exocytosis. Mol Pharmacol 67:1591–1599.

Herring BE, McMillan K, Pike CM, Marks J, Fox AP, Xie Z (2011) Etomidate and propofol inhibit the neurotransmitter release machinery at different sites. J Physiol 589:1103–1115.

Herring BE, Xie Z, Marks J, Fox AP (2009) Isoflurane inhibits the neurotransmitter release machinery. J Neurophysiol 102:1265–1273.

Hines AD, van Swinderen B (2021) Tracking single molecule dynamics in the adult *Drosophila* brain. eNeuro 8:ENEURO.0057-0021.2021.

Holt M, Varoqueaux F, Wiederhold K, Takamori S, Urlaub H, Fasshauer D, Jahn R (2006) Identification of SNAP-47, a novel Qbc-SNARE with ubiquitous expression*. J Biol Chem 281:17076–17083.

Jan LY, Jan YN (1976) L-glutamate as an excitatory transmitter at the *Drosophila* larval neuromuscular junction. J Physiol 262:215–236.

Jaqaman K, Loerke D, Mettlen M, Kuwata H, Grinstein S, Schmid SL, Danuser G (2008) Robust single-particle tracking in live-cell time-lapse sequences. Nat Methods 5:695–702.

Jones MV, Harrison NL, Pritchett DB, Hales TG (1995) Modulation of the GABAA receptor by propofol is independent of the gamma subunit. J Pharmacol Exp Ther 274:962.

Jung S, Zimin PI, Woods CB, Kayser EB, Haddad D, Reczek CR, Nakamura K, Ramirez JM, Sedensky MM, Morgan PG (2022) Isoflurane inhibition of endocytosis is an anesthetic mechanism of action. Curr Biol 32:3016–3032.e3.

Kádková A, Radecke J, Sørensen JB (2019) The SNAP-25 protein family. Neuroscience 420:50–71.

Karunanithi S, Cylinder D, Ertekin D, Zalucki OH, Marin L, Lavidis NA, Atwood HL, van Swinderen B (2020) Proportional downscaling of glutamatergic release sites by the general anesthetic propofol at *Drosophila* motor nerve terminals. eNeuro 7:ENEURO.0422-0419.2020.

Kasula R, et al. (2016) The Munc18-1 domain 3a hinge-loop controls syntaxin-1A nanodomain assembly and engagement with the SNARE complex during secretory vesicle priming. J Cell Biol 214:847–858.

Kim JJ, Gharpure A, Teng J, Zhuang Y, Howard RJ, Zhu S, Noviello CM, Walsh RM, Lindahl E, Hibbs RE (2020) Shared structural mechanisms of general anaesthetics and benzodiazepines. Nature 585:303–308.

Koyanagi Y, Torturo CL, Cook DC, Zhou Z, Hemmings HC (2019) Role of specific presynaptic calcium channel subtypes in isoflurane inhibition of synaptic vesicle exocytosis in rat hippocampal neurones. Br J Anaesth 123:219–227.

Lai Y, et al. (2017) Molecular mechanisms of synaptic vesicle priming by Munc13 and Munc18. Neuron 95:591–607.e10.

Li CH, Tam PKS (1998) An iterative algorithm for minimum cross entropy thresholding. Pattern Recognit Lett 19:771–776.

Liu W, Wilson R (2013) Glutamate is an inhibitory neurotransmitter in the *Drosophila* olfactory system. Proc Natl Acad Sci U S A 110:10294–10299.

Lor C, Perouansky M, Pearce RA (2020) Isoflurane potentiation of GABA(A) receptors is reduced but not eliminated by the beta3(N265M) mutation. Int J Mol Sci 21:9534.

Maidorn M, Olichon A, Rizzoli SO, Opazo F (2019) Nanobodies reveal an extra-synaptic population of SNAP-25 and syntaxin 1A in hippocampal neurons. MAbs 11:305–321.

Mandolesi G, Vanni V, Cesa R, Grasselli G, Puglisi F, Cesare P, Strata P (2009) Distribution of the SNAP25 and SNAP23 synaptosomal-associated protein isoforms in rat cerebellar cortex. Neuroscience 164:1084–1096.

Miesenböck G, De Angelis DA, Rothman JE (1998) Visualizing secretion and synaptic transmission with pH-sensitive green fluorescent proteins. Nature 394:192–195.

Molina-Obando S, Vargas-Fique JF, Henning M, Gür B, Schladt TM, Akhtar J, Berger TK, Silies M (2019) ON selectivity in the *Drosophila* visual system is a multisynaptic process involving both glutamatergic and GABAergic inhibition. Elife 8:e49373.

Morgan PG, Hoppel CL, Sedensky MM (2002) Mitochondrial defects and anesthetic sensitivity. Anesthesiology 96:1268–1270.

Nagele P, Mendel JB, Placzek WJ, Scott BA, D'Avignon DA, Crowder CM (2005) Volatile anesthetics bind rat synaptic snare proteins. Anesthesiology 103:768–778.

Ouyang W, Wang G, Hemmings HC (2003) Isoflurane and propofol inhibit voltage-gated sodium channels in isolated rat neurohypophysial nerve terminals. Mol Pharmacol 64:373.

Padmanabhan P, Bademosi AT, Kasula R, Lauwers E, Verstreken P, Meunier FA (2020) Need for speed: super-resolving the dynamic nanoclustering of syntaxin-1 at exocytic fusion sites. Neuropharmacology 169:107554.

Parslow A, Cardona A, Bryson-Richardson RJ (2014) Sample drift correction following 4D confocal time-lapse imaging. J Vis Exp 86:e51086.

Perouansky M, Johnson-Schlitz D, Sedensky MM, Morgan PG (2023) A primordial target: mitochondria mediate both primary and collateral anesthetic effects of volatile anesthetics. Exp Biol Med 248:545–552.

Ribrault C, Reingruber J, Petković M, Galli T, Ziv NE, Holcman D, Triller A (2011) Syntaxin1a lateral diffusion reveals transient and local SNARE interactions. J Neurosci 31:17590.

Rowe J, Calegari F, Taverna E, Longhi R, Rosa P (2001) Syntaxin 1A is delivered to the apical and basolateral domains of epithelial cells: the role of munc-18 proteins. J Cell Sci 114:3323–3332.

Ruiz-Montasell B, Aguado F, Majó G, Chapman ER, Canals JM, Marsal J, Blasi J (1996) Differential distribution of syntaxin isoforms 1A and 1B in the rat central nervous system. Eur J Neurosci 8:2544–2552.

Scheffer LK, et al. (2020) A connectome and analysis of the adult *Drosophila* central brain. Elife 9:e57443.

Shu T, Jin H, Rothman JE, Zhang Y (2019) Munc13-1 MUN domain and Munc18-1 cooperatively chaperone SNARE assembly through a tetrameric complex. Proc Natl Acad Sci U S A 117:1036–1041.

Speigel IA, Hemmings HC (2021) Selective inhibition of gamma aminobutyric acid release from mouse hippocampal interneurone subtypes by the volatile anaesthetic isoflurane. Br J Anaesth 127:587–599.

Speigel IA, Patel K, Hemmings HC (2022) Distinct effects of volatile and intravenous anaesthetics on presynaptic calcium dynamics in mouse hippocampal GABAergic neurones. Br J Anaesth 128:1019–1028.

Su Q, Mochida S, Tian JH, Mehta R, Sheng ZH (2001) SNAP-29: a general SNARE protein that inhibits SNARE disassembly and is implicated in synaptic transmission. Proc Natl Acad Sci U S A 98:14038–14043.

Südhof TC (2012) The presynaptic active zone. Neuron 75:11–25.

Sudhof TC, Rizo J (2011) Synaptic vesicle exocytosis. Cold Spring Harb Perspect Biol 3:a005637.

Tinevez J-Y, Perry N, Schindelin J, Hoopes GM, Reynolds GD, Laplantine E, Bednarek SY, Shorte SL, Eliceiri KW (2017) Trackmate: an open and extensible platform for single-particle tracking. Methods 115:80–90.

Tomlin SL, Jenkins A, Lieb WR, Franks NP (1998) Stereoselective effects of etomidate optical isomers on gamma-aminobutyric acid type A receptors and animals. Anesthesiology 88:708–717.

Ton HT, Phan TX, Abramyan AM, Shi L, Ahern GP (2017) Identification of a putative binding site critical for general anesthetic activation of TRPA1. Proc Natl Acad Sci U S A 114:3762–3767.

Torturo CL, Zhou Z-Y, Ryan TA, Hemmings HC (2019) Isoflurane inhibits dopaminergic synaptic vesicle exocytosis coupled to Ca V 2.1 and Ca V 2.2 in rat midbrain neurons. eNeuro 6:ENEURO.0278-0218.2018.

Troup M, Tainton-Heap LAL, van Swinderen B (2023) Neural ensemble fragmentation in the anesthetized *Drosophila* brain. J Neurosci 43:2537–2551.

Troup M, Zalucki OH, Kottler BD, Karunanithi S, Anggono V, van Swinderen B (2019) Syntaxin1a neomorphic mutations promote rapid recovery from isoflurane anesthesia in *Drosophila melanogaster*. Anesthesiology 131:555–568.

Ullrich A, Böhme MA, Schöneberg J, Depner H, Sigrist SJ, Noé F (2015) Dynamical organization of syntaxin-1A at the presynaptic active zone. PLoS Comput Biol 11:e1004407.

van Swinderen B, Kottler B (2014) Explaining general anesthesia: a two-step hypothesis linking sleep circuits and the synaptic release machinery. Bioessays 36:372–381.

van Swinderen B, Saifee O, Shebester L, Roberson R, Nonet ML, Crowder CM (1999) A neomorphic syntaxin mutation blocks volatile-anesthetic action in *Caenorhabditis elegans*. Proc Natl Acad Sci U S A 96:2479–2484.

Verderio C, et al. (2004) SNAP-25 modulation of calcium dynamics underlies differences in GABAergic and glutamatergic responsiveness to depolarization. Neuron 41:599–610.

Vrontou E, Groschner LN, Szydlowski S, Brain R, Krebbers A, Miesenbock G (2021) Response competition between neurons and antineurons in the mushroom body. Curr Biol 31:4911–4922.e4.

Wallis TP, et al. (2023) Super-resolved trajectory-derived nanoclustering analysis using spatiotemporal indexing. Nat Commun 14:3353.

Wang H-Y, Eguchi K, Yamashita T, Takahashi T (2020) Frequency-dependent block of excitatory neurotransmission by isoflurane via dual presynaptic mechanisms. J Neurosci 40:4103.

Woll KA, et al. (2016) A novel bifunctional alkylphenol anesthetic allows characterization of γ-aminobutyric acid, type A (GABAA), receptor subunit binding selectivity in synaptosomes*. J Biol Chem 291:20473–20486.

Woll KA, Guzik-Lendrum S, Bensel BM, Bhanu NV, Dailey WP, Garcia BA, Gilbert SP, Eckenhoff RG (2018) An allosteric propofol-binding site in kinesin disrupts kinesin-mediated processive movement on microtubules. J Biol Chem 293:11283–11295.

Xie Z, McMillan K, Pike CM, Cahill AL, Herring BE, Wang Q, Fox AP (2013) Interaction of anesthetics with neurotransmitter release machinery proteins. J Neurophysiol 109:758–767.

Xue M, Zhang B (2002) Do SNARE proteins confer specificity for vesicle fusion? Proc Natl Acad Sci U S A 99:13359–13361.

Yang J, Jin H, Liu Y, Guo Y, Zhang Y (2022) A dynamic template complex mediates Munc18-chaperoned SNARE assembly. Proc Natl Acad Sci U S A 119:e2215124119.

Zalucki OH, Menon H, Kottler B, Faville R, Day R, Bademosi AT, Lavidis N, Karunanithi S, van Swinderen B (2015) Syntaxin1A-mediated resistance and hypersensitivity to isoflurane in *Drosophila melanogaster*. Anesthesiology 122:1060–1074.

Zecharia AY, et al. (2012) GABAergic inhibition of histaminergic neurons regulates active waking but not the sleep-wake switch or propofol-induced loss of consciousness. J Neurosci 32:13062–13075.

Zhang M, et al. (2012) Rational design of true monomeric and bright photoactivatable fluorescent proteins. Nat Methods 9:727–729.

Zhou C, Johnson KW, Herold KF, Hemmings HC (2019) Differential inhibition of neuronal sodium channel subtypes by the general anesthetic isoflurane. J Pharmacol Exp Ther 369:200–211.

Zimin PI, Woods CB, Kayser EB, Ramirez JM, Morgan PG, Sedensky MM (2018) Isoflurane disrupts excitatory neurotransmitter dynamics via inhibition of mitochondrial complex I. Br J Anaesth 120:1019–1032.

Zimin PI, Woods CB, Quintana A, Ramirez JM, Morgan PG, Sedensky MM (2016) Glutamatergic neurotransmission links sensitivity to volatile anesthetics with mitochondrial function. Curr Biol 26:2194–2201.